Saturated and vadose zone fate and transport of a continuously released tracer in a sub-arctic bog peatland

by

Nicole Balliston

A thesis

presented to the University Of Waterloo

in fulfillment of the

thesis requirement for the degree of

Master of Science

in

Geography (Water)

Waterloo, Ontario, Canada, 2017

Author's Declaration

This thesis consists of material all of which I authored or co-authored: See Statement of Contributions included in the thesis.

This is a true copy of the thesis, including any required final revisions, as accepted by my examiners.

I understand that my thesis may be made electronically available to the public.

Statement of Contributions

This thesis is structured in accordance with the manuscript option. Chapters Two and Three will be submitted for review, as such, the published papers may differ from the chapters presented here based on the comments from the peer review process.

Nicole Balliston designed and executed the experiments and collected the resulting data. Nicole Balliston wrote the first draft of all chapters herein, where Dr. J. Price, who acted as the advisor for this thesis, provided editorial comments on each chapter or manuscript. As the thesis advisor, Dr. Price provided guidance on the research approach, field methods, experimental design, and comments and suggestions in the writing. Dr. C. McCarter provided guidance on the experimental design for the field and laboratory experiments, and Dr. R. Simhayov provided guidance on the experimental design for the laboratory experiment.

Abstract

In Ontario's James Bay Lowland, sub-arctic bog and fen peatlands make up 90% of the landscape. Increasing resource extraction operations in this area pose a risk of contaminant release into these systems, both intentional (i.e. high nitrogen/ sulphate/ phosphate wastewater outputs) and unintentional (i.e. crude oil pipeline leakages, fuel carrying train derailments, etc.). Once released, there is potential for solute migration and accumulation through both saturated and unsaturated transport processes. Further, capillary action has the potential to mobilize contaminants upwards towards the non- vascular mosses which dominate the surface. The limited existing field and laboratory studies have only provided preliminary information on fate and transport of dissolved solute, and no field studies have considered the potential accumulation of solute above the water table in a bog peatland. In the event of a release, a thorough understanding of solute fate and transport within the saturated and unsaturated (vadose) zones is necessary to predict the fate of the plume and the potential impacts on peatland ecosystems.

To better understand contaminant transport in these systems, approximately 14 000 L/day of sodium chloride (300 mg/L) was released into a bog in the James Bay Lowland. The tracer was pumped into a fully penetrating well (1.5 m below ground surface (bgs)) over a 45 day period in 2015 between July 5 and August 18. Plume development was measured in the saturated zone via in situ specific conductance (SC), temperature, and water table depth from a well and piezometer monitoring network. Specific conductance measurements were collected in the unsaturated zone using Time Domain Reflectrometry (TDR) sensors installed at 5, 10, and 15 depths (cm bgs). Meteorological data were collected from nearby weather stations for the duration of the spill. Following the spill, four 30 cm long cores were extracted from the site. An unsaturated breakthrough experiment was conducted for 60 days in a laboratory setting using a

300 mg/L sodium chloride solution, to verify processes observed in the field. Depth dependent soil parameterization was completed on each core following this experiment to determine the influence of inter core heterogeneity on unsaturated solute distribution.

In the saturated zone, over the spill period the bulk of the plume travelled a lateral distance of 100 m in the direction of a slight water table gradient (0.004 m/m). The plume shape was irregular and indicative of preferential flow paths formed by interconnected hollows in the landscape. Saturated transport of the tracer occurred primarily within the 25 cm piezometers (corresponding to the acrotelm). A discontinuous second high hydraulic conductivity layer at ~125 cm bgs also experienced rapid solute advection. Transport was confounded by a large amount of precipitation (233 mm total over the study period), which enhanced lateral dispersion, and diluted the tracer in the highly conductive upper peat layer. Solute also showed the potential to accumulate and remain in lower hydraulic conductivity hummocks adjacent to flow paths, and potentially within closed pores in the peat matrix. These results highlight the complexity of fate and transport in bog peatlands, and the susceptibility of the systems in a real-world spill scenario as detailed knowledge about depositional environment, meteorological conditions, topography, water table gradient and contaminant specific behaviour are required for accurate plume assessment.

Field scale characterization of the vadose zone showed a strong dependence of unsaturated solute accumulation on hydrological conditions. In particular, elevated water table conditions increased connectivity between unsaturated hummocks and the saturated zone, greatly accelerating the rate of solute accumulation. Heterogeneity in soil structure increased the complexity of this relation, as less dense soil transmitted solute well under high water contents but did not retain the solute in low water content conditions. Denser soil experienced solute

accumulation at a slower place but had a greater water and solute retention capacity, better facilitating capillary rise and long term accumulation. In laboratory conditions inter core heterogeneity played a great role in solute accumulation. Rates of evaporation differed between cores; highest evaporative rates and upward solute mobility were noted in a core with a highly porous upper 5 cm underlain by dense peat, which supplied solute and retained water well above the water table. The results of this study highlight the importance of extracting samples representative of site conditions due to a large amount of inter-core heterogeneity. Further development of these concepts is recommended through the use of 2D unsaturated zone modelling.

Acknowledgements

I would like to provide thanks to my colleagues at the Wetlands Hydrology Lab, for continuously providing their friendship and support, and for broadening my knowledge and scientific perspective. In particular, I would like to thank Dr. Colin McCarter, Dr. Rubi Simhayov, and James Sherwood for providing their assistance and a practical foundation from which my research grew. Also, a huge thank-you to Dr. Jonathan Price for providing me with the opportunity of a lifetime, for his expert guidance, and for continuously pushing me to become a better scientist. This was truly the most worthwhile and life changing endeavour in my academic career.

I would also like to thank those I had the pleasure of working with at the De Beers Group of Companies Victor Diamond Mine, who supported me through an eventful field season and in many ways sparked my passion for preserving the beauty of the North. I would like to thank my friends and family back home, who listened to my endless rants and Eureka moments, and who helped me to find the confidence to always keep going. And finally, I would like to thank my wonderful life partner, Lauren Smith, who has always been a positive force in my life. Thank you for your undying optimism, for helping me keep my head high, and for reminding me to take care of myself as well as my research.

Dedication

Dedicated to my amazing partner Lauren Smith; I truly could not have done this without you.

Table of Contents

List of Figures

1 Introduction

With the continued discovery of mineral resources in Canada's James Bay Lowland (JBL), resource extraction and transportation activities are increasing. As a result, there is growing risk of contaminant release into the sub-arctic bog and fen peatlands, which shape the landscape in this area (Riley, 2011). Contaminant releases can be unintentional, such as crude oil leakage from pipelines or fuel (diesel) spills via train derailments, or intentional, such as the addition of phosphate, sulphate and nitrogen rich wastewater from mining camps.

Once released into these systems, there is potential for solute migration and accumulation within the variably saturated upper zone, both through saturated and unsaturated transport, which creates the potential for contaminant movement into fens or local surface water systems. Further, near surface accumulation of contaminants may have potential toxicity to the non-vascular living mosses at the surface (Pouliot *et al*., 2012; Rezanezhad *et al*., 2012). In general, subsurface transport and fate of released contaminants in sub-arctic bog peatlands is currently poorly understood and essentially undocumented.

The James Bay Lowland is located with the larger Hudson Bay Lowland, the second largest wetland complex in the world (Gorham, 2008). Sub-arctic bog and fen peatlands, which make up 90% of the JBL landscape (Riley, 2011), are defined by an accumulation of at least 40 cm of peat (National Wetlands Working Group, 1997). Bogs are ombrogeneous (precipitation fed) and have near surface waters which are acidic and low in dissolved minerals. Bog surface cover is dominated by mosses such as *Sphagnum* with some trees and ericaceous shrubs (National Wetlands Working Group, 1997). Fens are characterized by precipitation, groundwater and surface water inputs and thus have a dissolved mineral content ranging from poor to rich. Fens

poor in dissolved minerals have vegetation similar to bogs, while mineral rich fens are generally dominated by sedges and shrubs as well as mosses (National Wetlands Working Group, 1997).

The upper, variably saturated layer of a peatland soil profile, termed the acrotelm (Ingram, 1978), is composed of living vegetation and poorly decomposed organic material (Boelter, 1965). Underlying this is the fully saturated and more decomposed catotelm (Ingram, 1978). The lateral and vertical movement of water (and therefore solute) is complex due to the high degree of spatial heterogeneity (i.e. microtopography and depth dependent properties), and the site specific hydrological conditions at the time of the spill (i.e. water table elevation, water content and precipitation events). Existing studies only provide a preliminary understanding of the fate and transport of dissolved solute in both saturated and unsaturated media.

Saturated contaminant transport in bog peatlands can be described by a combination of advection, dispersion and diffusion, in conjunction with contaminant specific behaviours such as sorption, which may retard or enhance contaminant movement (Hoag & Price, 1995). The layered nature of hydraulic conductivity in peat combined with a shallow water table results in a predominance of advective transport within the acrotelm (~ top 50 cm) (Deiss *et al.*, 2004; Hoag & Price, 1995; McCarter & Price, 2017a). The heterogeneous hummock/ hollow topography may form preferential advective pathways through the hollows, as flow may be restricted by the ridges formed by hummocks (Price & Maloney, 1994).Variations in peat thickness, as well as presence of roots and other vegetation, further increases the variability of solute advective and dispersive behaviour (Baird, 1997; Beckwith *et al.*, 2003; Deiss *et al.*, 2004; Rezanezhad *et al.*, 2012). A combination of dispersion and diffusion into dead-end or closed pores contributes to retardation of contaminant flow, asymmetry in contaminant plume development, and tailing of contaminant concentrations over time (Hoag & Price, 1997; Hoag & Price, 1995; Rezanezhad *et*

al., 2012). High water tables increase the transmissivity of the acrotelm and promote lateral flow, while low water table conditions may result in a relative increase in vertical percolation (McCarter & Price, 2017a). Precipitation may also dilute solute concentrations in the acrotelm, while evapotranspiration may concentrate the solute. Existing field studies only provide a preliminary understanding of the relation between peat structure and the fate and transport of dissolved solute. An increased understanding of how peatland hydrology and peat structure controls the nature and extent of solute transport is required to properly characterize real-world spill scenarios.

The upper, variably saturated acrotelm (Ingram, 1978) has a network of large, open and connected pores that readily transmit flow under saturated conditions (Boelter, 1965). Studies have shown that in the acrotelm layer the majority of saturated flow (50-99%) is conducted through pores > 75 µm in diameter (Baird, 1997; Quinton *et al.*, 2009; Rezanezhad *et al.*, 2010). Between the surface and 30 cm below ground surface (cm bgs), total porosity can decrease by up to 20% and effective porosity by 80% (to ~0.10) while bulk density can more than double (Hoag & Price, 1997; Carey *et al.*, 2007). This vertical trend, as well as past evidence of intermittent high hydraulic conductivity layers at lower depths, alters the saturated and unsaturated hydraulic conductivity, and the water retention abilities of the soil, creating a complex vertical profile.

Water can be mobilized upwards from the saturated zone through the unsaturated zone via evapotranspiration and capillary rise towards the non-vascular *Sphagnum* mosses at the surface (Hayward & Clymo, 1982). This process has the potential to transmit dissolved solutes within the active pore spaces above the water table. As in the saturated zone, solutes may accumulate in the unsaturated zone via diffusion from mobile to immobile phases. However, the

presence and extent of diffusion depends on the structure and state of decomposition of the peat, as moderately decomposed *Sphagnum* peat may have less inactive porosity (Simhayov, 2017). Reactive solutes such as cations may further accumulate as they adsorb to the peat (McCarter & Price, 2017b; Rezanezhad *et al.*, 2016, 2012; Simhayov, 2017). The drop in water content with distance above the saturated zone decreases the maximum radius of pores which remain saturated and thus increases the tortuosity of the interconnected pore spaces, increasing mechanical dispersion. While solute ions remain dispersed and trapped in the peat matrix, the evaporation of water from the surface may result in evaporative accumulation, increasing the breakthrough rate compared to saturated transport (Simhayov, 2017). There is currently a dearth in knowledge regarding the movement and accumulation of solute above the water table in natural peat, at both laboratory and field scales.

1.1 Objectives

The overall goal of this research is to increase understanding of how peatland hydrology and peat structure controls solute transport in the saturated and vadose zones, and to investigate the potential for contaminants to migrate to the living, growing *Sphagnum* at the surface of the acrotelm. The specific objectives are to:

a) Determine the spatial and temporal evolution of a developing contaminant (solute) plume in the saturated zone
b) Distinguish the effects of meteorological conditions and regional groundwater flow gradients on plume movement and distribution
c) Determine the ability of *Sphagnum* hummocks to accumulate and retain solute above the water table under field conditions, and relate solute accumulation to depth and variability of the water table and volumetric soil water content.

d) Relate the hydraulic structure and physical properties of peat and *Sphagnum* mosses to the plume's distribution through the site and down the peat profile

1.2 Organization of Thesis

This thesis consists of four chapters in line with the manuscript option at the University of Waterloo. Chapter 1 provides a general introduction to the research, including the large-scale processes and concepts, background information and the objectives of the thesis.

Chapters 2 and 3 are the results and analysis of a field scale solute transport experiment in a sub-arctic bog. Saturated zone transport processes are discussed in Chapter 2 (objectives a, b and d), whereas upper partially saturated zone processes are detailed in Chapter 3 (objectives c and d). Chapter 3 also details an unsaturated zone breakthrough experiment conducted in the laboratory, and the detailed analysis of soil physical properties in the top 30 cm of the peat profile (objectives c and d).

Chapter 4 provides a synthesis of the conclusions and recommendations for future research.

Appendix A, located at the end of the thesis, provides detailed results of statistical analysis completed for various mathematical relationships developed throughout the thesis.

2 Continuous sodium chloride tracer release and saturated zone plume development at a sub-arctic bog in the James Bay Lowland, Ontario

2.1 Introduction

With the mineral resources in Canada's James Bay Lowland (JBL), extraction and transportation activities are on the rise. Consequently, there is an increasing risk of contaminant release into sub-arctic bog and fen peatlands, which dominate the landscape in this area (Riley, 2011). Contaminant releases can be unintentional (i.e. crude oil leakage from pipelines or fuel (diesel) spills via train derailment), or intentional (i.e. phosphate, sulphate and nitrogen rich wastewater from mining camps). Subsurface transport and fate of released contaminants in sub-arctic bog peatlands is currently poorly understood and essentially undocumented, largely due to a lack of field-scale research. Only one field experiment has been conducted in a bog (Hoag & Price, 1995), however the spill was instantaneous and not ideal for tracking long term solute behaviour.

The James Bay Lowland is a subsection of the Hudson Bay Lowland, which is the second largest wetland complex in the world (Gorham, 2008); in this area bog and fen peatland complexes cover up to 90% of the landscape (Riley, 2011). Below the peat is a deposit of clay-sized marine sediment 8-30 m thick on average (with localized thicknesses up to several hundreds of meters) (HCl, 2004), underlain by the Silurian bedrock of the Upper and Lower Attawapiskat formation (Martini, 1981; McDonald, 1989). The fine-grained marine sediment has a low average hydraulic conductivity and thus acts as an aquitard on which the peat has accumulated (Whittington & Price, 2012).

Bog and fen peatlands, defined by an accumulation of 40 cm or more of organic material (peat) are interconnected within this landscape; the ombrotrophic bogs store atmospheric water and release it through groundwater outflow to fens and surface water systems (National

Wetlands Working Group, 1997; Quinton *et al.*, 2003; Siegel & Glaser, 1987). Bogs are precipitation fed (ombrogenous), unlike fens which may have both ground and surface water connections. Further, near surface bog water is acidic and low in dissolved minerals (National Wetlands Working Group, 1997). Seasonal processes (i.e., spring melt) and precipitation events increase water table elevation and bog-fen connectivity (McCarter & Price, 2017a).

Bog vegetation is dominated by *Sphagnum* mosses due to the nutrient-poor and acidic conditions, with sparse growth of vascular vegetation in slightly more nutrient rich areas, such as along bog-fen or bog-surface water margins (Glaser *et al.*, 2004).

The soil structure of bog and fen peat has a number of physical and hydrological characteristics that influence water and thus dissolved solute flow. The peat profile is characterized by two distinct layers, a ~15 – 50 cm layer of living, poorly decomposed and variably saturated plant remains, termed the acrotelm, underlain by the perpetually saturated layer of more decomposed peat, called the catotelm (Ingram, 1978). Saturated hydraulic conductivity (K_{sat}) decreases by up to five orders of magnitude between the surface and the upper boundary of the catotelm, where it remains consistently low (Boelter, 1965). However, studies on extracted peat cores have shown the presence of unexpectedly high (Beckwith *et al.*, 2003) or low (McCarter & Price, 2017a) hydraulic conductivity layers below the acrotelm, suggesting a highly complex, heterogeneously layered subsurface.

Variation in *Sphagnum* species creates a diverse surface microtopography, complicating the hydraulic conductivity distribution. Species such as *Sphagnum fuscum* are smaller and grow in denser formations, better facilitating capillary rise of water above the water table (McCarter & Price, 2014). As a result they may form hummocks (high points), which can be up to ~40 cm above the average surface elevation (Andrus *et al.*, 1983). Other species such as *Sphagnum*

rubelleum and *Sphagnum majus* are larger and grow in less densely packed formations, resulting in flat areas or depressions in the topography where the water table is closer to the surface (Robroek *et al.*, 2007).

At the pore scale peat soil has a dual porosity structure composed of active (open and connected) and inactive (closed and dead end) pores; flow occurs through the active pores (Baird & Gaffney, 2000; Deiss *et al.*, 2004; Hoag & Price, 1995; Rezanezhad *et al.*, 2016). Macropores, or large interconnected pore spaces, have been shown to convey up to 80% of flow in saturated near surface peat, creating preferential flow pathways (Holden, 2009; Rezanezhad *et al.*, 2009). An increasing degree of decomposition and compaction with depth results in a decrease of the active porosity (% of pore spaces which are open and connected) and the average pore size, thus increasing the peat's water holding capacity and tortuosity (Quinton *et al*., 2009; Rezanezhad *et al.*, 2009; Weiss *et al*., 1998).

Saturated contaminant transport in soils can be described by a combination of advection, dispersion, and diffusion, in conjunction with contaminant specific behaviours such as sorption which may retard or enhance contaminant movement (Hoag & Price, 1995). To our knowledge, three field-scale solute transport experiments have been documented in peatlands, providing a general understanding of the controls on solute transport (Baird & Gaffney, 2000; Hoag & Price, 1995; McCarter & Price, 2017b). The layered nature of hydraulic conductivity in peat combined with a shallow water table results in a predominance of advective transport within the acrotelm (Deiss *et al.*, 2004; Hoag & Price, 1995, McCarter & Price, 2017b). The heterogeneous hummock/ hollow topography increases field-scale dispersion, and may form preferential advective pathways through the less densely packed hollows (Beckwith *et al.*, 2003; Boelter, 1965). These preferential pathways create a bypassing effect of solute flow, which may result in

retardation rates of <1 (solute flow greater than the average linear water velocity) (Baird & Gaffney, 2000). Heterogeneity caused by variations in peat thickness, as well as presence of roots and other vegetation, further increases the variability of solute advective and dispersive behaviour (Baird, 1997; Beckwith *et al.*, 2003; Deiss *et al.*, 2004; McCarter and Price, 2016; 2017b; Rezanezhad *et al.*, 2012). A combination of dispersion and diffusion into dead-end or closed pores contributes to retardation of contaminant flow, asymmetry in contaminant plume development and tailing of contaminant concentrations over time (Hoag & Price, 1997; Hoag & Price, 1995; Rezanezhad *et al.*, 2012).

Local hydrological conditions have an additional impact on field scale solute transport behaviour. High water table conditions increase the transmissivity of the acrotelm and promote lateral flow, while low water table conditions may result in lowered lateral flow and an increased potential for vertical percolation (McCarter & Price, 2017a). Precipitation may also dilute solute concentrations in the acrotelm, reversing concentration gradients between the acrotelm/ catotelm and open/ closed pores, resulting in solute tailing (Hoag & Price, 1995; Price & Woo, 1988; Price, 1994). Evapotranspiration (ET) may also concentrate the solute depending on time-scale, rate of flow, and relative contribution of ET to the water budget (Hoag & Price, 1995; Price, 1994; Simhayov, 2017).

Existing field studies only provide a preliminary understanding of the relation between peat structure and the fate and transport of dissolved solute. One field-scale experiment has been conducted in a bog (Hoag & Price, 1995), however it used surficial, instantaneous contaminant addition, which may not be ideal for tracking long term advective, diffusive and dispersive behaviours. The goal of this research is to increase understanding of how peatland hydrology and

peat structure controls the nature and extent of solute transport in a field setting using a continuous conservative solute injection. The specific objectives are to:

a) Determine the spatial and temporal evolution of a developing contaminant (solute) plume in the saturated zone of a sub-arctic bog
b) Relate the physical structure of peat and *Sphagnum* mosses to the plume's distribution through the site and down the peat profile
c) Distinguish the effects of meteorological conditions and regional groundwater flow gradients on plume movement and distribution

2.2 Study Site

The study site (Exp Bog) is a 4 500 m^2 section of a domed bog northwest of the De Beers Group of Companies Victor Diamond Mine (51°51'13"N, 83°56'26" W, 85 m asl) situated ~90 km west of Attawapiskat in the James Bay Lowland (Figure 2-1). The regional topography is flat, and the study site is on the margin of a domed bog; it slopes gently towards a stream. There is a distinct hummock hollow microtopography formed by the *Sphagnum* mosses, with greater surficial connectivity between adjacent hollows towards the north end of the site. The hummocks are 0.5 to 1.0 m in diameter and 10-15 cm high on average, with a contributing area of 1980 m^2 and 2520 m^2 for hummocks and hollows respectively, determined by manual in-field mapping. On-site observations confirm that *Sphagnum fuscum* and *S. rubellum* dominate the hummocks while *S. majus* dominates the hollows. A sparse cover of stunted 1-4 m high *Picea mariana* (black spruce) trees are found throughout the site, with a greater density to the south. Peat thickness measured from cores extracted from the site with a Russian corer varied between 1.25 to 2.15 m. Average January and July temperatures (1981-2010 climate normals) are -20.7 and 15.4°C at Moosonee (250 km southeast), and -22.4 and 17.1°C at Lansdowne House (300 km southwest). Average yearly precipitation (1981-2010 climate normals) at Moonsonee and

Lansdowne house is 700 mm and 681 mm, respectively, with 30% and 35% falling as snow, respectively (Environment Canada, 2015a; 2015b). During the ice-free season evapotranspiration is the dominant source of water loss, whereas groundwater outflow and surface runoff are generally minimal unless water table conditions are high and surface connectivity is advanced (Leclair, 2015; Perras, 2015).

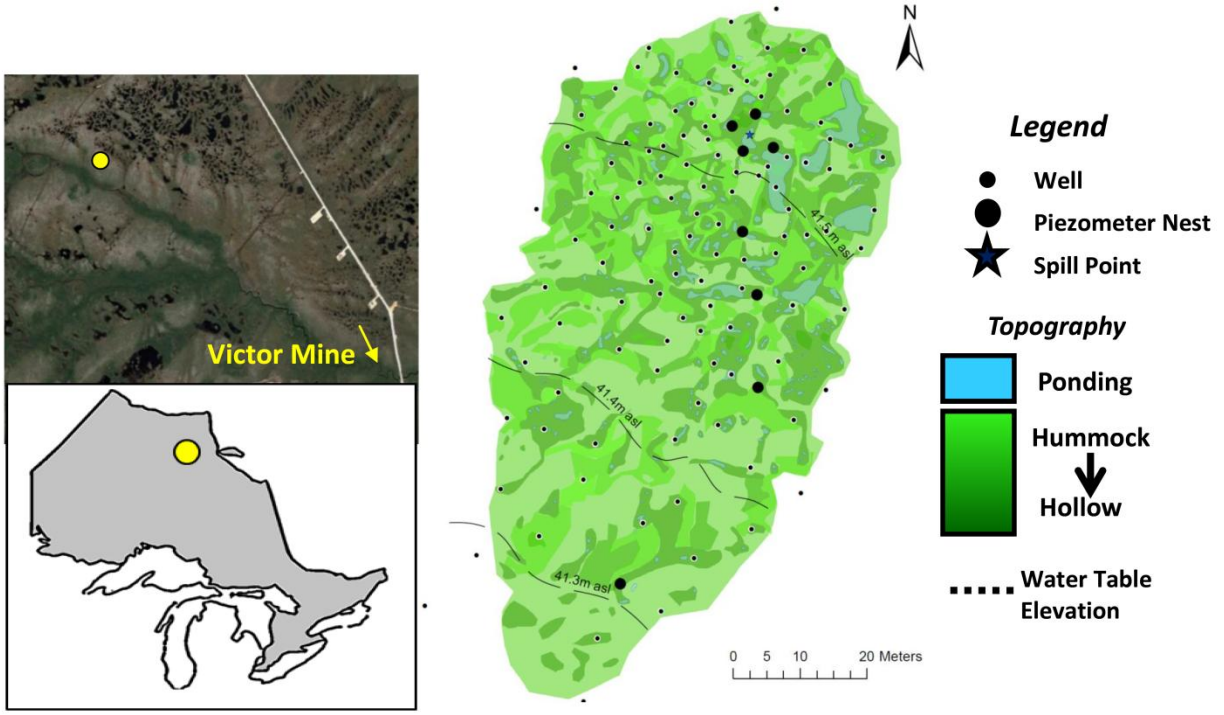

Figure 2-1 Location of the Experimental Bog (Exp Bog) in the James Bay Lowland (bottom left) relative to the De Beers Group of Companies Victor Diamond Mine (top left). Site water table, microtopography and well and piezometer installations are also shown (right).

2.3 Methods

The field solute injection experiment was conducted during the summer of 2015 over a 45-day period from July 5 (day 0) to August 18 (day 45). Actual injection began at 17:00 h on day 0. Background monitoring events took place between June 21 and July 1, 2015.

Precipitation totals were averaged every 20 minutes using a tipping bucket rain gauge (Texas Instruments TE525M-L tipping bucket rain gauge) installed at the Exp Bog and recorded

on a Campbell Scientific CR1000 data logger. Air temperature and relative humidity were recorded every 20 minutes with a HOBO Ux100-023 Temperature/RH Data Logger, located nearby (150 m NW). Net radiation (Q*) and ground heat flux (Q_G) were measured at the experimental fen using a net radiometer (REBS Q7.1 Net Radiometer) and a heat flux plate (REBS HFT3) recorded every 20 minutes on a Campbell Scientific CR1000 data logger. Gaps in precipitation, ground heat flux, and net radiation measurement were supplemented with hourly averages from the De Beers' weather station located ~2.5 km southeast of the study site.

Two bucket lysimeters were installed at one hummock and one hollow and were measured a minimum of twice weekly using a handheld electronic scale. Lysimeter ET values were used to calibrate the Priestley-Taylor combination model for actual ET using the fitted coefficient of evaporability (α) (Priestley & Taylor, 1972) such that

$$ET = \alpha \left[\frac{s}{(s+\gamma)}\right]\left[\frac{Q*-Q_g}{L_p\rho}\right] \qquad \textbf{Eq.2-1}$$

where s is the slope of the saturation vapour pressure- temperature curve (kPa/ °C), γ is the psychrometric constant (0.066 kPa/ °C at 20°C), $Q*$ is the net radiation (W/m^2), Q_g is the ground heat flux (W/m^2), L_v is the latent heat of vaporization (J/kg), and ρ is the density of water (kg/m^3). Total ET across the site was determined using an aerially weighted average of hummock and hollow (44% and 56%, respectively).

Groundwater data and samples were collected using a series of 1" PVC wells and piezometers which were slotted, screened with geotextile filter sock (Rice Engineering & Operating LTD., 2" Filter Sock) and sealed at the bottom. Wells were slotted over a 1.25 m interval and piezometers were slotted at a 0.2 m interval centered at the intended depth. Manual water table readings were taken at all wells daily during the first week of the spill and at increasing time intervals thereafter. Manual readings were supplemented with 12 Schlumberger

Mini-Diver D1501 level loggers (accuracy of ± 0.5 cm H_20) installed in 8 monitoring wells, averaged at 30-minute intervals.

To determine K_{sat}, bail tests were conducted at 36 monitoring wells and 8 piezometer nests during the first week following the solute injection period. At each location a Schlumberger Mini-Diver D1501 level logger was installed ~5 cm from the bottom of the pipe and logged at 0.1 to 1 second intervals, depending on well response rate. A volume of water was removed quickly using Waterra^{TM} foot-valve and tubing to achieve a minimum of 20 cm drawdown. The water level was then left to recover until a minimum of 90% recovery was achieved. The data were then used to calculate K_{sat} using Hvorslov's (1951) hydrostatic time-lag method.

Sodium chloride (NaCl) was used as the solute tracer due to its relatively non-reactive nature and its ease of in-field measurement through the surrogate measure of electrical conductivity (EC), which can be temperature corrected to 25°C to yield specific conductance (SC) (Hoag & Price, 1995) where

$$SC = \frac{EC}{1+(0.019*(T-25)} \qquad \textbf{Eq.2-2}$$

where EC is the measured electrical conductivity (µS/cm) and T is the temperature of the water (°C).

A concentrated solution of sodium chloride (Solution A, see Figure 2-2) was prepared in a 210 L barrel adjacent to the spill point to obtain a concentration of ~30 g NaCl/L. The solution was mixed hourly using a bilge pump (Attwood Rsunami T-500, 500 gph) to prevent stratification. This solution was pumped at a target rate of 150 L/day to an outflow weir bucket, where it mixed with fresh water for delivery to the bog. The barrel was fitted with a Schlumberger Mini-Diver D1501 level logger to record water stage at 30-minute intervals. A stage volume curve was generated to determine the real-time barrel-to-weir flow rate during the

45-day spill period. This was important as the actual rate of barrel-to-weir flow deviated from the 150 L/day target due to decreased effectiveness of the solute pump and occasional blockages which decreased the flow rate.

Fresh water was also delivered to the outflow weir by a solar powered pump (Lorentz PS150-Centric Submersible Pump) from a nearby bog pool complex (Solution B Figure 2-2). The fresh water was pumped to the outflow weir at a target rate of 15 000 L/day, diluting the NaCl concentration in the weir to a target of ~300 mg/L (Solution C Figure 2-2). Due to differences in molecular weight (chloride: sodium mass ratio of 1.5:1), this results in target chloride and sodium outputs of 182 and 118 mg/L respectively. The rate of diluted NaCl solution released from the bucket weir was measured with a V-notch fitted with a second Schlumberger Mini-Diver D1501 level logger transducer; a stage-discharge curve was used to estimate the average weir outflow at 30 minute intervals for the entire solute injection period. The pumping rate from the bog pond deviated from the 15 000 L/day target due to pump blockages and power availability, affecting the dilution ratio. Once exiting the bucket weir, the diluted NaCl solution was injected into a perforated 4” PVC well slotted to a depth of 1.5 meters below ground surface (m bgs).

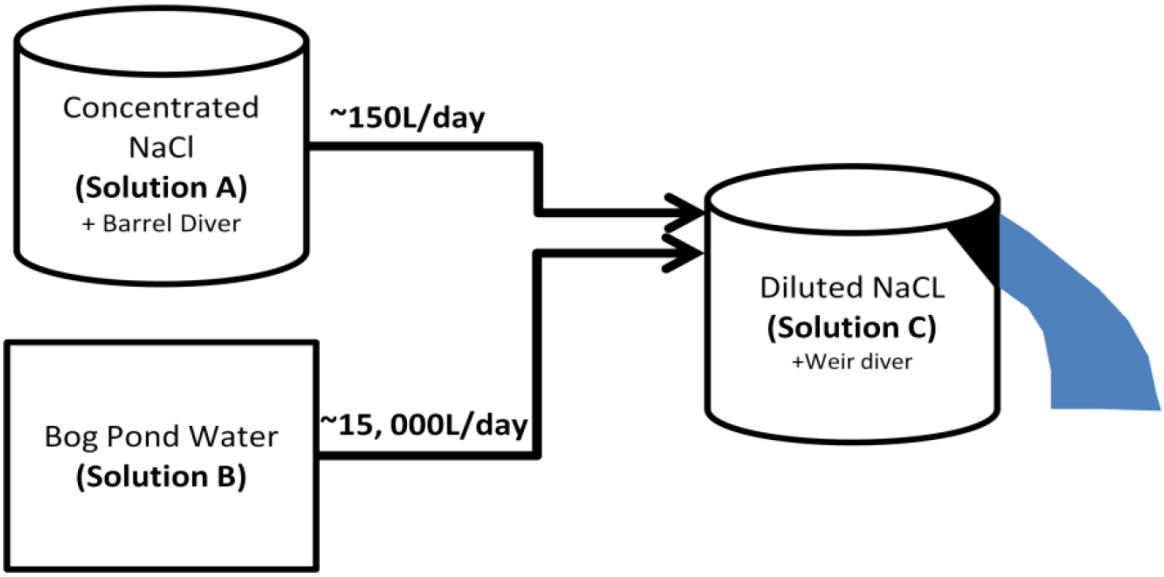

Figure 2-2 Schematic diagram of the instrumentation at the spill injection point. A concentrated sodium chloride solution (A) was mixed with pond water (B) to a NaCl concentration of ~300 mg/L at the outflow (C).

Due to the variability of both the barrel-to-weir flow and the bog pond-to-weir flow, the actual NaCl concentration in the weir outflow was not constant. The known NaCl concentration in the barrel, the barrel-to-weir flow rate, and the bog pond-to-weir flow rate were used to determine the hourly weir output SC to better contextualize plume behaviour. This was done using USGS PHREEQ-C modelling software.

A forward mixing simulation in PHREEQ-C used the five known parameters (input NaCl, NaCl flow rate and temperature, and output flow rate and temperature) to run a dilution calculation for each hour of the spill, producing hourly weir outflow SC values. Background concentrations of common ions, taken from 2014 bog pond data, were used in the dilution calculations to more accurately determine SC in the weir outflow. Background concentrations include chloride (0.72 mg/L), sodium (2.18 mg/L), potassium (0.56 mg/L), magnesium (0.38 mg/L) and calcium (3.27 mg/L).

Plume development was monitored downstream using water samples collected from the well and piezometer network. Piezometers were installed in nests at depths of 25, 50, 75 and 125 cm bgs. Specific conductance (SC) was used as a surrogate measurement of NaCl presence through the comparison of in-field measured values to background values. Specific conductance was calculated through in-field measurements of electrical conductivity (EC) using a handheld YSI probe, corrected to SC using field temperature also measured by the YSI. The implications of using SC to represent a solution that includes non-conservative cations (Na^+) are discussed later.

During each monitoring event, each pipe was purged three times and the sample was collected in a 100 mL graduated cylinder, into which the YSI probe was inserted for SC and temperature measurement. To determine a threshold for plume presence, 12 wells and 4 piezometer nests were installed and sampled on June 21, 27, 28 and July 1 to determine a background SC of 200 µS/cm. During the solute injection period, additional wells and piezometer nests were progressively installed in the anticipated direction of plume movement using the following methodology:

1. A small hole was dug at a "best-guess" location free of surface water, immediately surrounding the known plume extent
2. A water sample was withdrawn and SC was tested with the YSI field probe
3. If SC was elevated above the 200 µS/cm threshold a well and/ or piezometer nest was immediately installed at the location **OR**
4. If the SC was below the 200 µS/cm threshold the location was flagged and revisited during subsequent monitoring events.

The final monitoring network totaled 123 monitoring wells and 9 multi-level piezometer nests (Figure 2-1). The type of microtopography each well was installed into (i.e. hummock or hollow) was noted in-field, and later used to determine hummock hollow well pairings.

2.4 Results

2.4.1 Hydrology

The study site experienced an unusually wet summer season. Between July 5 and August 19, 233 mm of precipitation fell at the site (Figure 2-3) compared to the July-August combined climate normal of 175 mm (1981-2010) (Environment Canada, 2015a; 2015b). Of the 45 days, 25 experienced rainfall events, 7 of which the total exceeded 15 mm. Values of α used to calculate actual ET were determined to be 0.72 and 0.67 for hummocks and hollows, respectively (see Figure A-1 in Appendix). Over the 45-day period ET remained fairly constant compared to precipitation, totalling 65 mm with an average of 1.4 mm/day.

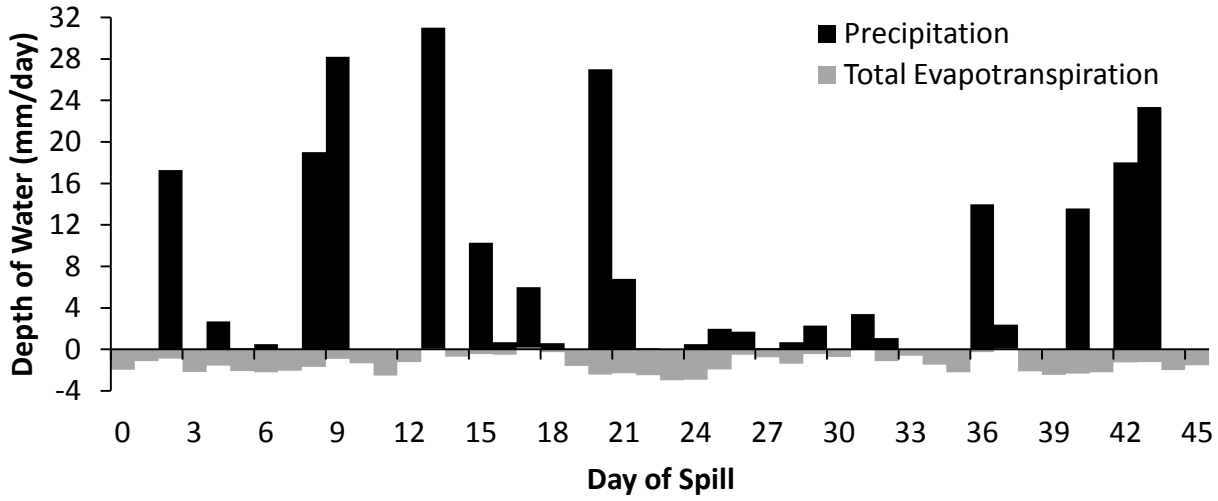

Figure 2-3 Daily rates of precipitation (black) at the study site as well as the total daily evapotranspiration from the spatially weighted hollows and hummocks (grey).

Over a north-south transect along the site (100 m) the average water table elevation decreased by ~0.4 m (Figure 2-1). During the first week of the spill and before the first major rainfall event on day 8, the average groundwater elevation in the vicinity of the injection point

was 84.8 m asl (Figure 2-4), which on average is within 10 cm of the ground surface. After the large rainfall events on days 8 and 9 the water table elevation increased by ~7 cm, which created ponded conditions in the hollows of the landscape, which remained present for the remainder of the spill due to the numerous subsequent rainfall events (Figure 2-1). Ponding was the most evident within a 25 m arc downstream of the injection point due to a combination of the pumping input and to the higher density of hollows in this area, however isolated ponding was observed over the entire site. Sporadic measurements of ponded water at affected monitoring wells confirmed that surficial and subsurface SC was equivalent where ponding was present. Water table levels fluctuated by ~5 cm for the remainder of the spill due to numerous smaller rainfall events; however the lowest recorded water table level after these rainfall events was still ~2 cm above the pre day 8/9 rainfall values.

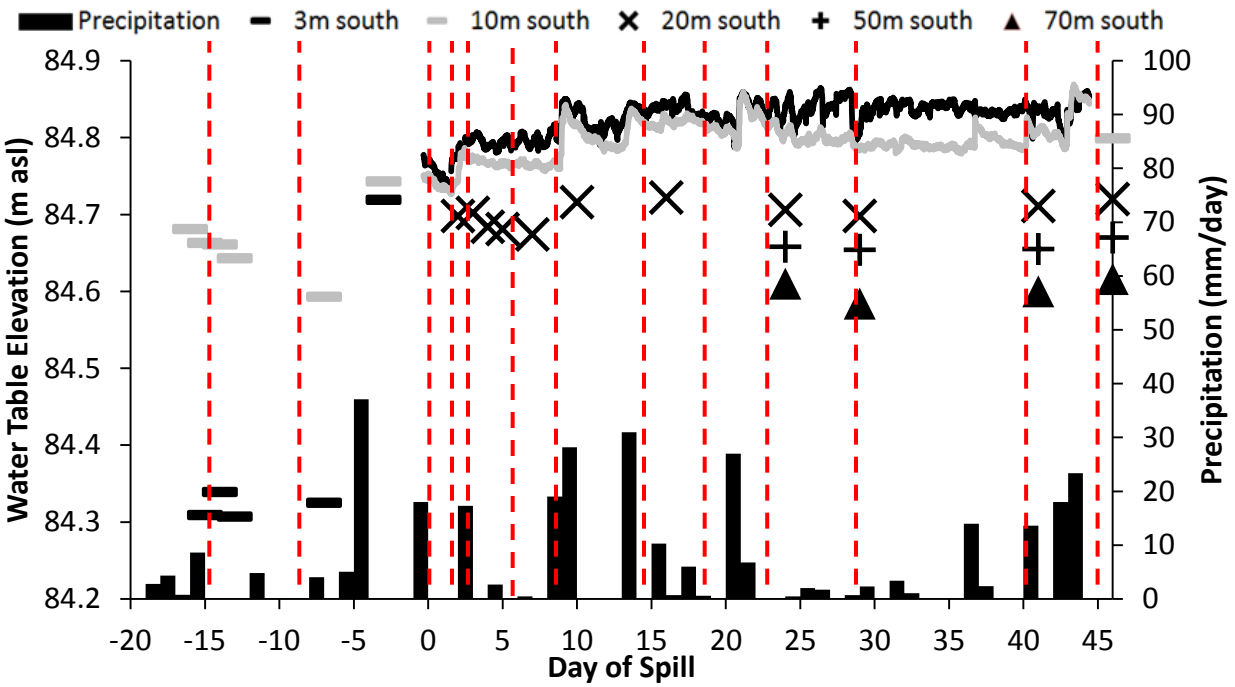

Figure 2-4 Daily precipitation (secondary y axis) and water table elevation 3, 10, 20, 50 and 70 m from the injection point. Continuous lines represent data taken from water level loggers calibrated with manual values, while points represent individual manual water table readings. Field measurements of SC are indicated with a dashed red line.

The geometric average, maximum and minimum well K_{sat} values were 2.5, 21.6 and 0.13 m/day (Figure 2-5). Piezometer nest hydraulic conductivity profiles showed a great deal of vertical and lateral variability. In all piezometer nests, K_{sat} was greatest at the 25 cm depth, corresponding to the acrotelm (Figure 2-5). There was also at least an order of magnitude decrease in K_{sat} at all piezometer nests between the 25 cm and the 50 cm depths. K_{sat} increased between the 75 cm and 125 cm piezometers at five of eight nests (1, 2, 3, 7 and 9).

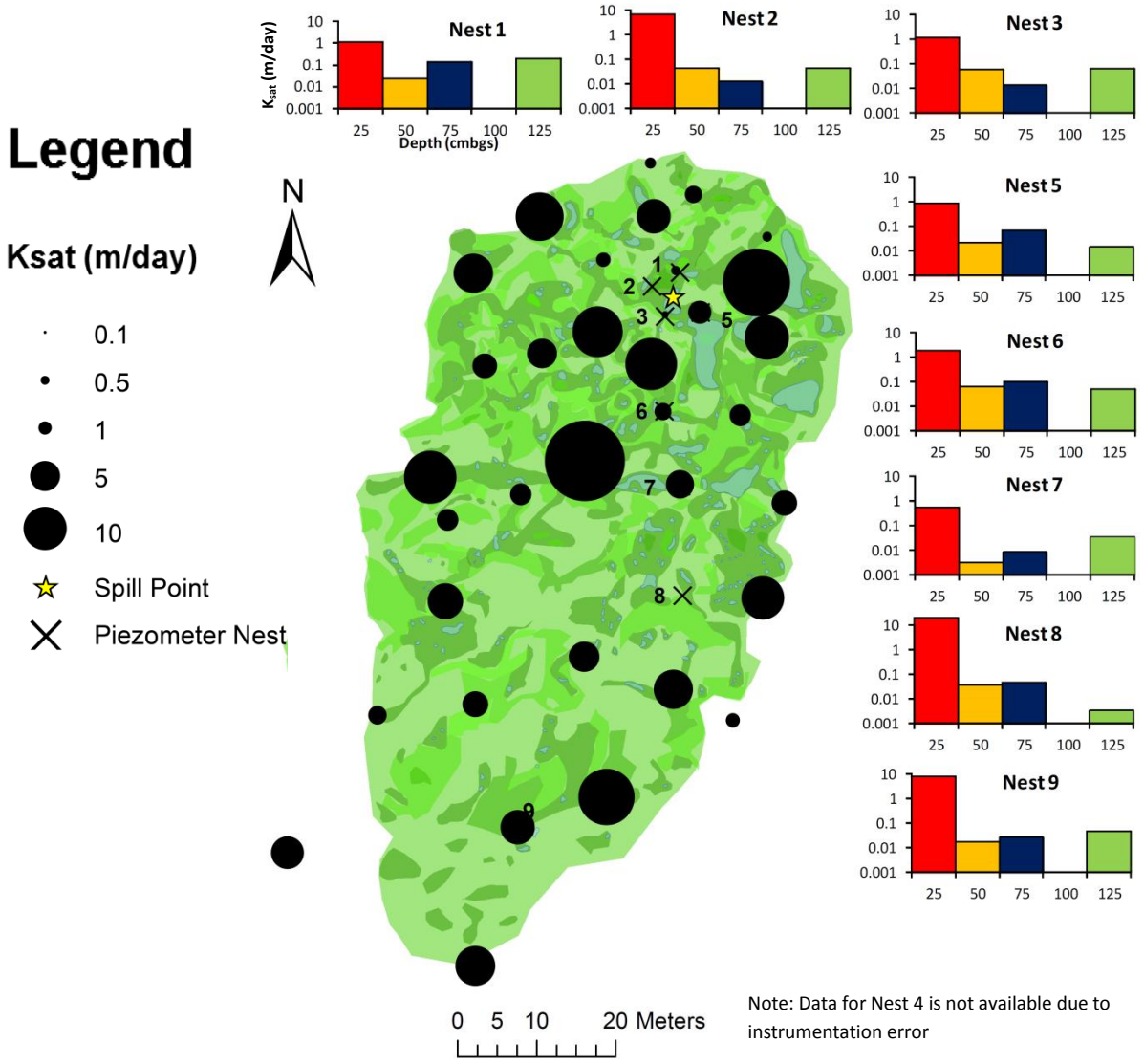

Figure 2-5 Site layout showing piezometer nest locations and scaled results of full well hydraulic conductivity (K_{sat}) tests. The surrounding graphs show results from piezometer nest (25, 50, 75, 125 cm) K tests.

Comparing K_{sat} between the 16 wells installed in hummocks versus the 15 wells installed in hollows (Figure 2-6) the geometric mean is not significantly different (2.3 and 2.8 m/day respectively). However, K_{sat} values in hollow wells have a much larger range of values, and a much greater maximum (21.6 m/day and 9.3 m/day respectively).

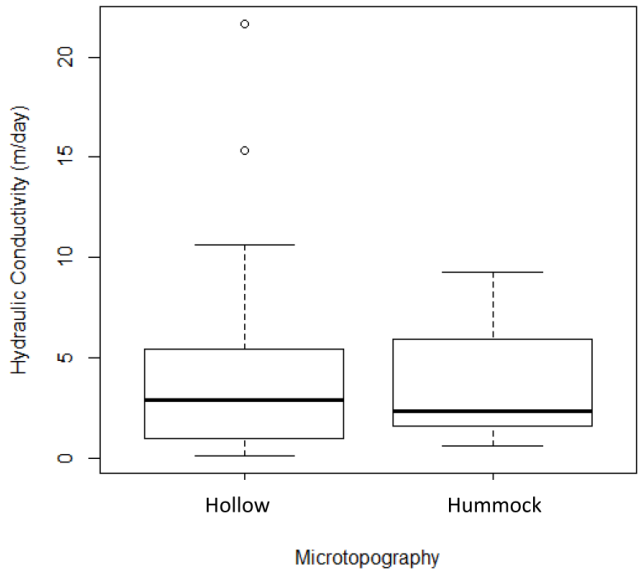

Figure 2-6 Box plots showing the median, first and third quartiles, and range of K_{sat} values between the 16 wells located in hummocks and the 15 wells located in hollows.

2.4.2 Solute Transport

A total of 113 kg of NaCl were added to the site during the 45 day solute injection period, with an average SC of 543 µS/cm, an average solute input rate of 13 500 L/day, and an average mass flux of 2.7 kg NaCl/day. Solute input rates, mass loading, and SC, were highly variable at both hourly and daily timescales (Figure 2-7). Variation in both water and solute input were due to changing water levels in the intake pond, solar power availability for both the inflow and solute pumps, and equipment malfunction such as solute pump clogging and corrosion.

Specific conductance contours were generated from 12 monitoring events (Figure 2-8). Over the spill injection period the plume front advanced a total of 100 m (average of ~2 m/day). The predominant direction of plume movement was to the south; after rapid plume development

during the first 24 hours in all directions the plume spread only 2.5 m in the east and west directions, and 5 m in the north direction by day 45. In the dominant flow direction, a fingering of the plume emerged by day 10, and a second by day 20. These fingers continued to develop through day 45, effectively bisecting the south end of the plume into two.

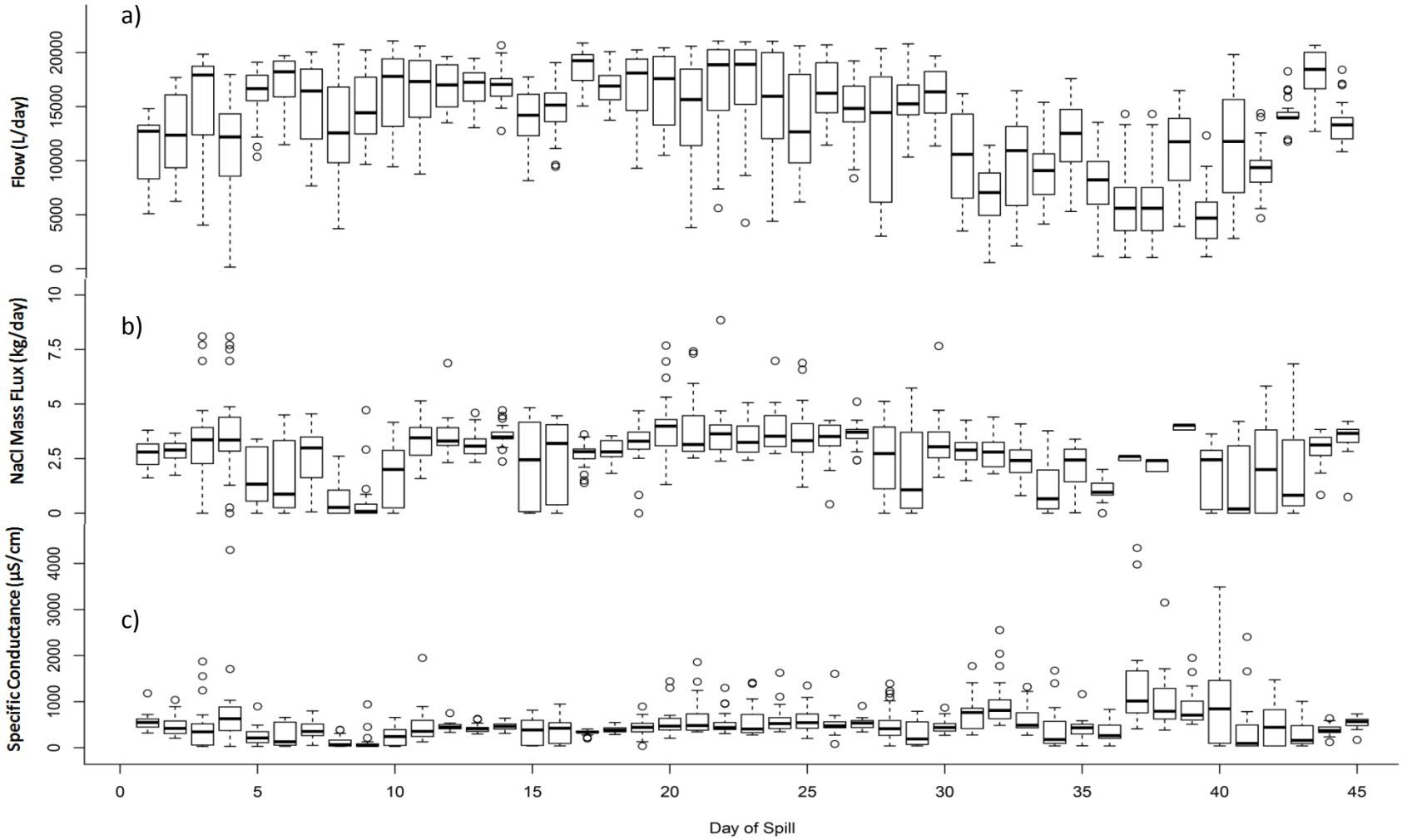

Figure 2-7 Boxplots summarizing data averaged hourly from (a) solute flow into the injection well measured using an outflow weir transducer (b) NaCl mass flux using known barrel concentration and outflow rates (c) outflow SC using PHREEQ-C forward mixing simulation. Boxes show the 1st 2nd (median) and 3rd quartiles while the "whiskers" represent the maximum and minimum hourly values.

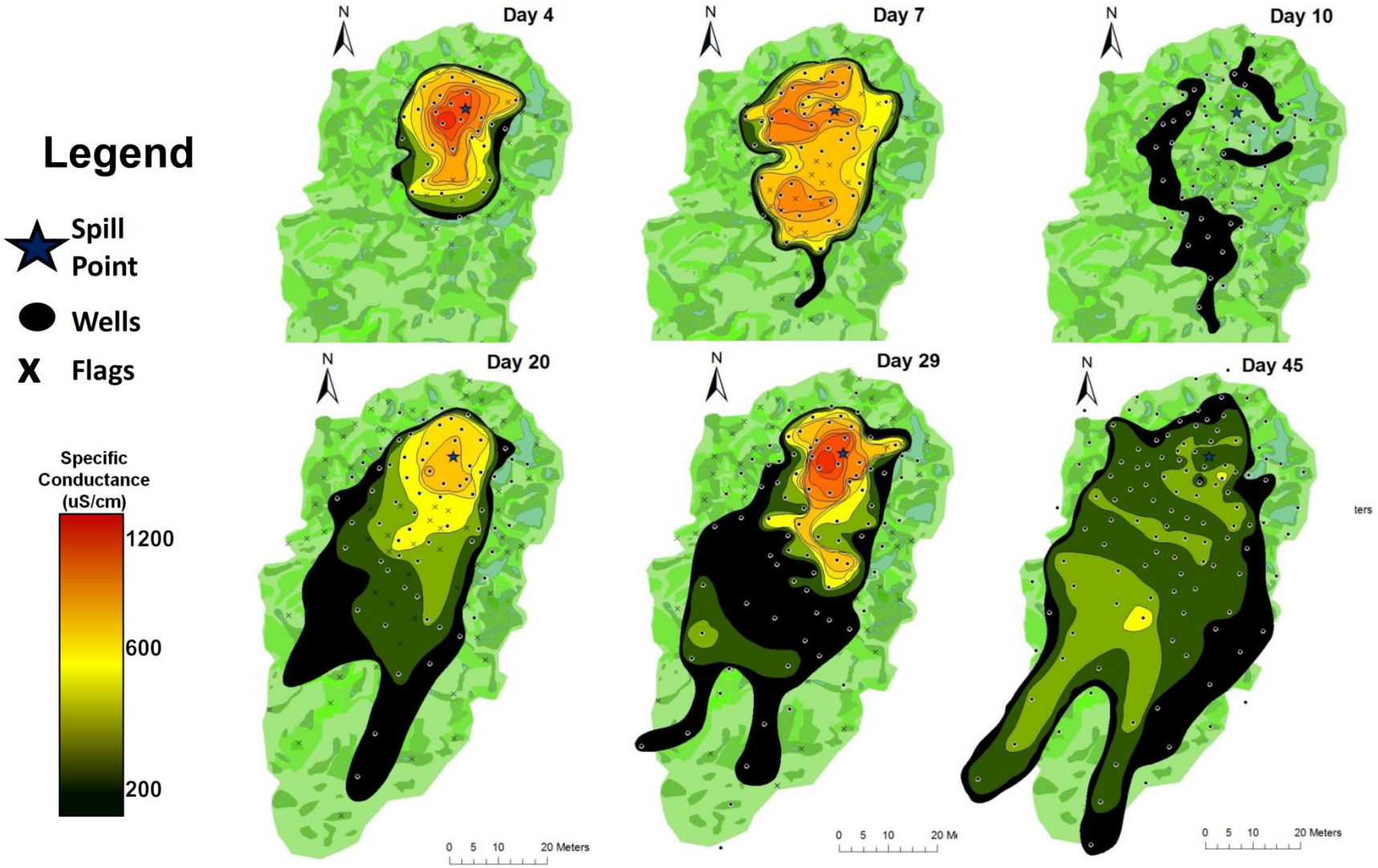

Figure 2-8 Specific conductance (SC) contours generated on days 4, 7, 10, 20, 29, and 45 of the injection period. Wells and flags used to generate the contours using in-field measurements are included on each sub-map.

There were some periods during the spill when no advance was measured. In fact, between days 20 and 24, the apparent position of the plume front moved in the north direction (towards the injection point) at a rate of 3.25 m/day (not shown); this occurred at the same time as the day 8/9 rain event. To a lesser degree this apparent recession can also be observed between days 7 and 10, where the plume SC dropped below the background threshold over the majority of the plume area, followed by a re-establishment by day 20.

Fluctuations of SC over the spill period varied between paired hummock and hollow wells (Figure 2-9). At the three paired hummock/hollow wells (left) the hollows initially experienced a greater increase in SC than the associated hummocks. However by day 45, SC values decreased more rapidly in the hollows and the relationship reversed. In the non hummock and hollow pairings this pattern was not observed; the paired wells' SC did not differ notably, and there were no apparent trends with lateral distance from the injection point.

Vertical distribution of the solute was highly variable with time and with distance from the injection well, although patterns in piezometer nest SC did correlate well with the SC contours (Figure 2-10). The three piezometer nests (1, 2 and 3) that were installed prior to the spill had background SC values below the 200 µS/cm threshold at all screened depths. At Day 0 these values immediately jumped to reflect SC values in the wells. For the duration of the spill the 25 cm and 125 cm depths correlated best with well SC (Figure 2-10). The 25 cm piezometer correlated best with well SC at Nest 2 ($p<0.001$, adj $R^2=0.99$), Nest 6 ($p<0.001$, adj $R^2=0.90$), and to a lesser degree Nest 3 ($p<0.001$, adj $R^2=0.56$). The 125 cm piezometer SC correlated best with well SC at Nest 1 ($p<0.001$, adj $R^2=0.71$), Nest 3 ($p<0.001$, adj $R^2=0.76$), and to a lesser degree Nest 6 ($p<0.01$, adj $R^2=0.50$). Simple linear regression was not conducted on Nests 7, 8 and 9 due to their small sample size (<5), however visual observation of Nests 8 and 9 suggests a

greatest correlation between the well SC values and those in the 25 cm layer. No statistically significant correlations between well SC and piezometer SC were determined at other layers.

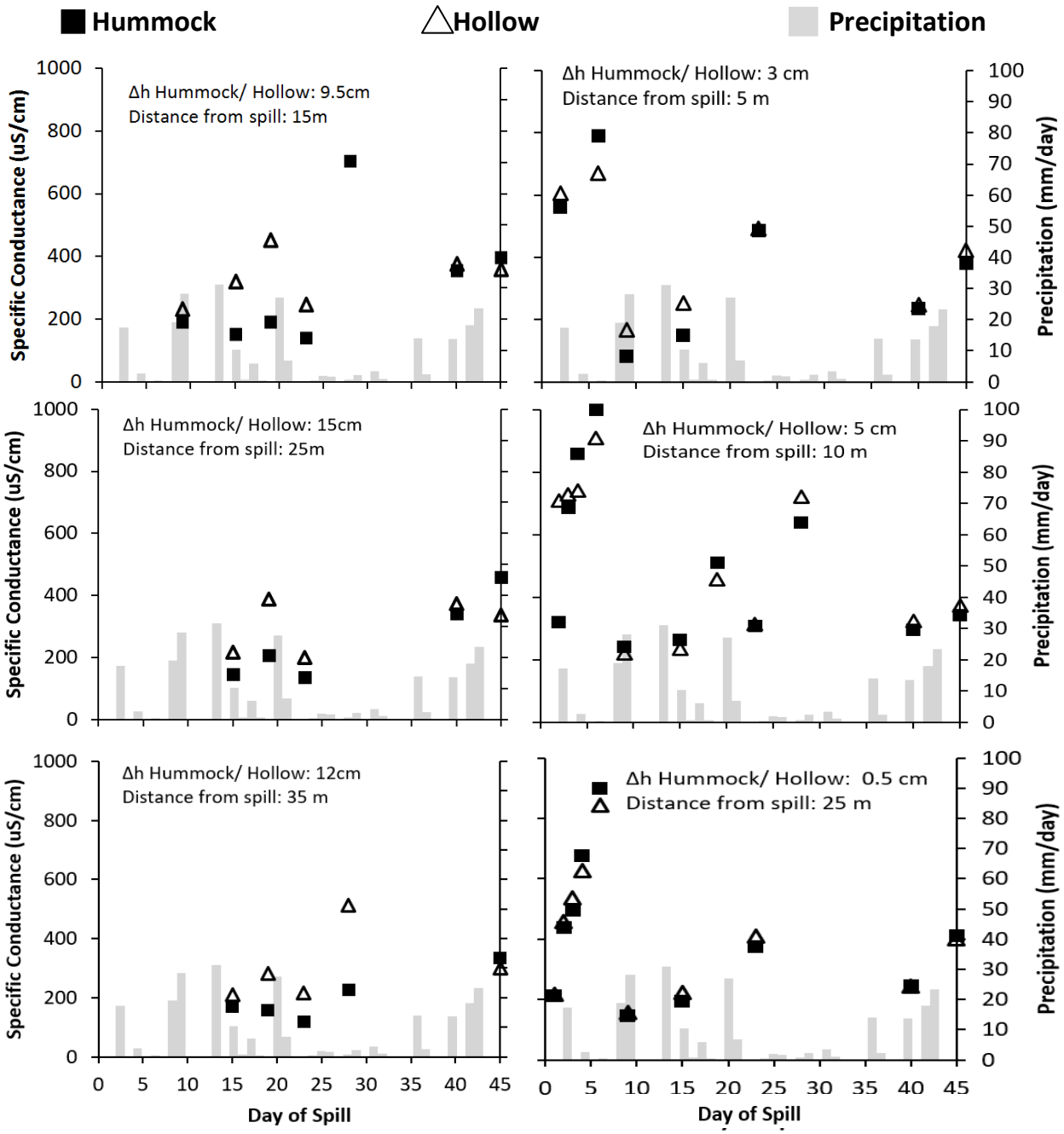

Figure 2-9 SC readings and precipitation at paired hummock (squares) and hollow (triangles) wells for the duration of the spill period (left) as well as paired wells nearly equivalent in microtopography (right). Each well in a pairing are located roughly equidistant from the spill point and <5 m from one another.

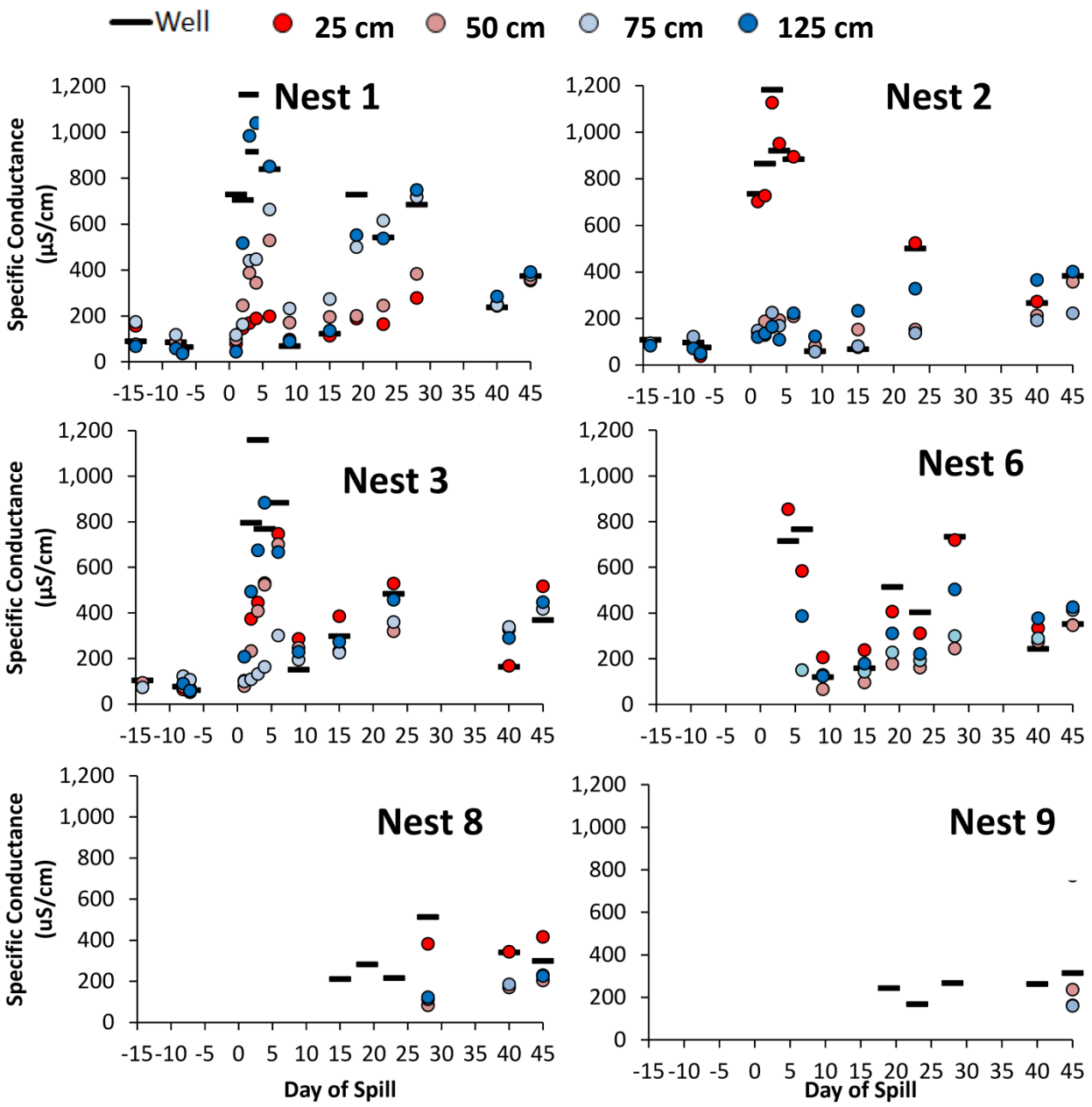

Figure 2-10 SC readings at selected piezometer nests (25, 50, 75, 125 cm) over the background monitoring and solute injection period. Also included are the SC readings at the wells associated with each piezometer nest.

2.5 Discussion

Plume behaviour was influenced by a dynamic interplay of input variability, meteorological conditions, and the hydraulic structure of the bog. The local water table gradient was the driving force for plume movement and shape, being enhanced by the hydrological forcing caused by the pumped inflow (McCarter & Price, 2017a). While a localized groundwater mound around the injection point resulted in some up-gradient migration of the solute, the plume developed predominantly to the south, which corresponds to the site-wide hydraulic gradient of 0.004 (m/m) in this direction (Figure 2-1 groundwater contours, Figure 2-8 SC contours). There was considerable transverse spreading of the plume; the length/width ratio on day 4 and 45 were 1:1 and 3:1, respectively. This is in contrast to that of a NaCl plume generated by an "instantaneous" release in a blanket bog (Hoag & Price, 1995) in which the hydraulic gradient was 0.055, compared to 0.004 in this study (and the length/width ratio was 35:1 after 30 days). Here, the localized groundwater mound resulting from the continuous release, coupled with the lower hydraulic gradient, resulted in more transverse spreading. As a consequence, the plume in this study was forced to pass through a greater range of local microtopography, which probably reduced the flow rate and increased solute dispersion on account of the increased tortuosity of the flowpath.

The maximum recorded rate of plume front advancement (~20 m/day) was in the first 24 hours and attributable to groundwater mounding, as shown by a ~2-3 cm jump in water table level at 3 and 7 m from the injection point (Figure 2-4). After this point the daily rates of plume front movement were highly variable. Differences in lateral hydraulic conductivity across the site affected plume front advection as it migrated southwards due to a heterogeneous and complex subsurface environment. This is consistent with past field scale experiments (Hoag & Price, 1995; McCarter & Price, 2017b).

Peak SC values were consistently observed along a narrow central conduit as early as day 7 (Figure 2-8), suggesting that advection occurred along a preferential flow pathway. This resulted in an asymmetrical and fingered plume shape, which split into two distinct fingers by day 20, persisting until the final monitoring event. These preferential pathways correspond to the interconnected series of hollows in the landscape, which allow lateral flow through the near surface acrotelm rather than be limited by slower hollow-to-ridge flow found in past studies (Price & Maloney, 1994). Many of these hollows had some degree of ponding for the duration of the spill (Figure 2-1), although most were not surficially connected due to the presence of the hummocks. In this experiment the average and minimum K_{sat} values were similar for the hummocks and the hollows, but maximum K_{sat} was much greater in hollows (Figure 2-6) than in hummocks. The four wells with highest K_{sat} (21.6, 15.3, 10.6 and 8.5 m/day) were located in hollows, three of which were along the advective pathway of the plume (Figure 2-5). The fourth, located east of Nest 5, was likely inflated due to the presence of a large amount of ponded water directly adjacent to the well, as the screen was slightly above the surface. The elevated K_{sat} in these wells, and likely the adjacent areas, results in linear pore water velocities an order of magnitude higher than the average.

As in previous field studies (Hoag & Price, 1995; McCarter & Price, 2017b), the bulk of plume advection occurred within the top 35 cm (Figure 2-10). This can be deduced from the statistically significant correlation between full well SC and the 25 cm piezometer SC in Nests 2, 3, 6, and the visual correlation at Nests 8 and 9. This, and the lack of visual connection between ponded areas, suggests the top 35 cm of peat was responsible for most solute transport. This is consistent with the high lateral hydraulic conductivity values at this depth (Figure 2-5), which

are typically one to two orders of magnitude greater at the 25 cm piezometers than at the corresponding 50, 75, and 125 cm piezometers within the same nest.

At piezometer Nests 1 and 3, and to a lesser degree 6, the 125 cm piezometer correlated to well SC, suggesting this layer also contributes to plume advection. At Nests 1, 2, 3, 7 and 9, there is notable increase in hydraulic conductivity at the 125 cm piezometer, suggesting a discontinuous higher hydraulic conductivity layer at this depth. This is consistent with observations at a nearby ribbed fen made by McCarter and Price (2017a), where a higher hydraulic conductivity layer about this depth also caused solute to diverge into deeper peat**.** Visual observations of relatively poorly decomposed peat with woody material were recorded at this depth during well and piezometer installation. This vertical plume divergence was not observed by Hoag and Price (1995), where the catotelm peat was consistently of low hydraulic conductivity and without distinct layering. However, their study was a single (non-continuous) surface release, whereas in this study, the 1.5 m injection well penetrated this higher hydraulic conductivity layer, delivering solute at depth (see elevated SC at 125 cm in Nest 1, immediately after the spill; Figure 2-10). However, since the higher hydraulic conductivity layer at 125 cm was common but not continuous (Figure 2-5), SC distribution at this depth was inconsistent. This complex heterogeneous vertical peat profile, and the preferential advection of solute through interconnected hollows, highlights the difficulty in predicting solute behaviour in field environments.

The multiple layers of high hydraulic conductivity, and the presence of large precipitation events during the spill period, were responsible for the apparent waxing and waning of the plume. Specifically, apparent plume recession occurred between days 7 and 10, and days 20 and 24 (Figure 2-8). This corresponds with large rainfall events on days 8/9 and day 20, which

increased water table elevation and diluted solute concentrations at the surface. When water samples were then collected from the wells after a rainfall event, the majority of collected water originated from the diluted layer, effectively masking solute presence. This can be related to the increase in water table height during rainfall events on day 8/9, and 20 (Figure 2-4), which are then reflected in a decreased SC in wells and highly correlated piezometers during monitoring events on days 9 and 23 (Figure 2-10). As the water table dropped after these events the dilutive effects were reduced, resulting in an increase of SC at the monitoring events on days 15 and 27.

Dispersion caused additional spreading of the plume and development of plume shape. Evidence of dispersion was noted in movement between the acrotelm and catotelm in Hoag and Price (1995). Evidence of dispersive mixing between the higher and lower conductivity layers was also observed at some piezometer nests (Figure 2-10). In particular, in Nests 3, 6 and 8 the slow, near linear increase in SC in the 50 and 75 cm piezometers suggests continuous ingress of solute into these layers, independent of the day to day fluctuations present in the advection-dominated layers.

Diffusive exchanges of solute between closed and open pores and sodium adsorption likely played a lesser role, but probably caused some solute retardation. Although sodium and chloride were not analyzed separately, there is evidence in past research of sodium and potentially chloride sorption (McCarter, 2017b). Retardation factors in this past study on average were 1.1 and 2.0 for chloride and sodium, respectively. The fact that the retardation factor for chloride, a non-reactive tracer, was greater than 1.0 suggests the presence of physical diffusion into inactive pores (Hoag & Price, 1997; Rezanezhad *et al.*, 2012). The greater retardation factor for sodium is likely due to the influence of sorption in addition to physical diffusion (McCarter & Price, 2017b).

Differences between hummock and hollow SC may be explained by the differences in soil physical properties. There is evidence that hummocks have a higher bulk density near the surface than hollows (Baird *et al.*, 2016). For this reason hollows more effectively convey solute, shown by the larger presence of elevated SC in hollow wells compared to the paired hummocks for the majority of the spill (Figure 2-9). However, hummocks have greater water retention due to the smaller pore sizes, and a greater capacity for solute diffusion into closed pores. Therefore while the SC in the hollows was diluted due to the precipitation event on day 40, the solute which had accumulated in the hummocks was better retained, creating the SC trend reversal on day 45 in the three hummock and hollow well pairs.

Field scale experiments must consider methodological and analytical errors, as well as how spatial and temporal sampling variability affect interpretations. Solute input flow rates, mass loading rates, and therefore SC values were inconsistent, creating alterations in plume shape. For example, interruptions in pumping between days 4 and 7 resulted in a smeared plume shape with a second plume "center" not associated with the injection well (Figure 2-8). Further, during the first 7 days of the spill injection period the SC values recorded using the YSI probe exceeded the input SC values within 10 m of the injection well. This discrepancy is also noted between the YSI values and those recorded by the four conductivity loggers at piezometer Nests 1-5, suggesting YSI measurement error. This error could not be reproduced and corrected using the YSI in laboratory conditions. This has implications on the magnitude of plume contours during this 7 day period, as the error may have falsely inflated SC measurements during this time.

Upwelling of solute from the mineral layer underlying the peat could not be confirmed via groundwater sampling. Water levels in all piezometer nests indicated downward hydraulic

gradients only. Upward hydraulic gradients, and therefore upwelling of ions from mineral soils in bog peatlands is not expected in this area (Leclair, 2015).

The use of SC as an indirect measure of NaCl, though convenient, introduces inherent flaws in measurement. Most importantly, the presence of Cl^-, which is a conservative tracer, in contrast to Na^+, which is delayed by adsorption, was not accounted for in the SC measurements. It is likely that sodium remained in a closer radius to the injection point while chloride was predominately responsible for the majority of plume advection. This was reported in the study conducted by McCarter and Price (2017b) where the retardation factors for sodium and chloride were 2.0 and 1.1 respectively, resulting in much higher Cl^- concentrations 100 m downstream from the spill point (~40 mg/L) compared to Na^+ (~15 mg/L) by day 42.

Findings of this research are undeniably biased by a wetter than average season and the resulting presence of high water table conditions, which is known to increase hydrological connectivity of the system (McCarter & Price, 2017a). Lower water table conditions result in a less saturated acrotelm, eliminating saturated flow from the upper, most hydraulically conductive peat and thus lowering the transmissivity. This would likely result in a slower rate of plume progression and an increasing importance of unsaturated processes.

2.6 Conclusions

Transport of solute (NaCl) was influenced by a combination of peat structure and hydrological conditions. The plume travelled 100 m over the 45-day period exhibiting an elongated shape in the dominant direction of flow. Advection was predominately to the south, corresponding to a slight (40 cm) decrease in water table elevation. Lateral plume advection was preferential through interconnected hollows in the landscape. Vertically, advection occurred both in 25 cm piezometers, corresponding to the acrotelm, and in a second discontinuous high conductivity layer approximately 125 cm bgs. High water tables facilitated the saturation of the

acrotelm, enhancing advection in this layer by increasing its transmissivity (McCarter & Price, 2017a). Deeper advection in the 125 cm discontinuous layer corresponds to fibrous undecomposed woody material found at this depth. Large rainfall events resulted in periods of plume "masking" due to the dilution of solute in the upper, highly conductive layer. Vertical mixing transported solute into lower hydraulic conductivity areas, resulting in lower but more stable solute presence in hummocks versus hollows.

The overall fate and transport of contaminants in bog peatlands is complex, difficult to estimate and measure, and may have implications on the susceptibility of these systems to real-world spills. A continuous spill has the potential to result in rapid advective transport even under regionally flat conditions, at unpredictable depths dictated by the heterogeneous depositional history of the area. Further, measurement timing may result in unrealistic samples due to the temporary ability of rainfall to mask plume presence. Solute also shows the potential to accumulate and remain in lower hydraulic conductivity hummocks adjacent to flow paths, and potentially within closed pores in the peat matrix. Reactive contaminants, such as those present in wastewater effluent, may further accumulate through sorption, and may result in the accumulation of nutrients, and change the nutrient poor, acidic conditions necessary for the existence of bog peatlands (McCarter, 2016).

A detailed record of the local watertable gradient and topography of the site would be useful in predicting the advective pathway of a solute plume. However, the rate of advection as well as the vertical distribution of solute within the peat profile are complex, and require in-depth knowledge of the hydrological conditions at the time of the spill (i.e., water table depth), the site-specific depositional environment, the type of contaminant (reactive/ nonreactive), and the depth of the spill.

3 Capillary Rise of Solute in Partially Saturated Surficial Peat Profiles

3.1 Introduction

Increasing extraction and transportation of mineral resources in the James Bay Lowland (JBL) region of Canada poses a risk of contaminant release into bog and fen peatlands, which dominate the sub-arctic landscape (Riley, 2011). Contaminant releases can be unintentional (i.e. crude oil leakage from pipelines or fuel (diesel) spills via train derailment), or intentional (i.e. nutrient elevated wastewater from mining camps). Once released into these systems, there is potential for solute migration and accumulation within the variably saturated upper zone, both through saturated (Chapter 2) and unsaturated transport. This has potential toxicity to the non-vascular living mosses at the surface (Rezanezhad *et al.*, 2102; Pouliot *et al.*, 2012), which receive water drawn to the surface from the water table via capillary action (McCarter & Price, 2014; Price *et al*., 2010). Contaminant transport within the variably saturated upper zone, in particular the presence of solute movement and accumulation due to capillary rise, is poorly understood and has received little attention, especially in undisturbed *Sphagnum* peat profiles.

Sub-arctic bog and fen peatlands, which make up 90% of the JBL landscape (Riley, 2011), are defined through an accumulation of at least 40 cm of organic material (National Wetlands Working Group, 1997). The upper, variably saturated layer of the soil profile, termed the acrotelm (Ingram, 1978), is composed of living vegetation and poorly decomposed organic material. It has a network of large, open and connected pores that readily transmit flow under saturated conditions (McCarter & Price, 2014; Goetz & Price, 2015). Underlying this is the fully saturated and more decomposed catotelm (Ingram, 1978). Studies have shown that in the acrotelm layer the majority of saturated flow (50-99%) is conducted through macropores (Baird, 1997; Quinton *et al.*, 2009; Rezanezhad *et al.*, 2010), which are defined as pores > 75 µm in diameter (Brewer, 1965). Total porosity (volumetric proportion of pore spaces) and effective

porosity (volumetric proportion of saturated pore spaces that conduct flow) are high near the surface (~90-95% and 60-85%, respectively) and bulk density is low (<0.1 g/cm^3) (Carey *et al.*, 2007; Hoag & Price, 1997; McCarter & Price, 2017b; Price & Whittington, 2010; Rezanezhad *et al.*, 2016). The transition from acrotelm to catotelm is marked by an increasing degree of decomposition (Hayward & Clymo, 1982) and soil compaction due to a combination of decomposition and the weight of overlying material (Quinton *et al.*, 2009). Between the surface and 30 cm below ground surface (bgs), total porosity can decrease by up to 20% (to ~0.75) and effective porosity by up to 80% (to ~0.10) while bulk density can more than double (Hoag & Price, 1997; Carey *et al.*, 2007). The saturated hydraulic conductivity in acrotelm peat is high ($1x10^{-2}$ to $1x10^{-3}$ m/s) compared to that in the catotelm ($1x10^{-4}$ to $1x10^{-6}$ m/s) due to the large average hydraulic pore radius (Carey *et al.*, 2007) and the lower proportion of closed and disconnected pores (Hoag & Price, 1997; Rezanezhad *et al.*, 2016). Further, the specific yield of the acrotelm is high and the water retention is low, as larger pores drain more readily (Price *et al.*, 2008). This inability to retain water results in a rapid decline in water content and a decrease in unsaturated hydraulic conductivity of up to five orders of magnitude with increasingly negative pore water pressure (Price *et al.*, 2008). These vertical trends cannot be assumed in all cases however, as recent studies have shown high layers of saturated hydraulic conductivity in deeper peat (Baird *et al.*, 2016).

Due to the high hydraulic conductivity of the acrotelm, most lateral water movement, and thus solute advection, occurs within the top 30 cm of the peat profile, depending on the position of the water table (McCarter & Price, 2017b). The lateral and vertical movement of water (and therefore solute) is complex. This is attributed to water table fluctuations and preferential flow pathways in the microtopography (McCarter & Price, 2017a; 2017b). Past studies have shown

lateral permeability can vary by orders of magnitude within a 5 m radius due to inconsistency in microforms (Baird *et al.*, 2016). Furthermore, pore scale changes in tortuosity decrease flowpath connectivity, thus enhancing dispersion (Vervoort & Cattle, 2003). Solute may also diffuse from the mobile zone (active pores) to immobile zone (inactive pores), which results in retardation of even conservative (non-reactive) solutes (Hoag & Price, 1997; McCarter & Price, 2017b; Rezanezhad *et al.*, 2012). Reactive solutes such as sodium are further attenuated through sorption onto the organics (Rezanezhad *et al.*, 2016; Rezanezhad *et al.*, 2012) resulting in a potentially high cation exchange capacity (Simhayov, 2017).

Water can be mobilized upwards from the saturated zone through the unsaturated zone via capillary rise, and towards surficial non-vascular *Sphagnum* mosses (Hayward & Clymo, 1982). The capillary rise process has the potential to transmit dissolved solutes within the active pore spaces. As in the saturated zone, solutes may accumulate in the unsaturated zone via diffusion from mobile to immobile phases (Simhayov, 2017). Reactive solutes such as cations may further accumulate as they adsorb to the peat (Rezanezhad *et al.*, 2012; 2016; McCarter, 2017b; Simhayov, 2017). The drop in water content with distance above the saturated zone decreases saturated pore radius and thus increases the tortuosity of the interconnected pore spaces, increasing mechanical dispersion. While solute ions remain dispersed and trapped in the peat matrix, the evaporation of water from the surface may result in evaporative accumulation, increasing the breakthrough rate compared to saturated transport (Simhayov, 2017).

The movement and accumulation of solute above the water table in natural peat, at both laboratory and field scales, is not well documented. Sodium chloride (NaCl) breakthrough experiments have been conducted under saturated conditions (Hoag & Price, 1997; Ours *et al.*, 1997; Price & Woo, 1988; Rezanezhad *et al.*, 2012), however only one experiment has been

executed in an unsaturated regime (Simhayov, 2017). This unsaturated transport experiment used homogenized moderately decomposed fen peat with the large inclusions removed, which does not adequately represent the layered heterogeneity of a natural peat profile. Therefore, the purpose of this research is to better understand the potential for contaminants in the saturated zone to migrate to the living, growing surface of a *Sphagnum* peat profile. The specific objectives are:

1. Determine the ability of *Sphagnum* hummocks to accumulate and retain solute above the water table under field conditions, and relate solute accumulation to depth and variability of the water table and volumetric soil water content
2. Replicate the vertical rise of solute in *Sphagnum* mesocosms taken from the field site, under controlled steady-state laboratory conditions, to illustrate the nature and extent of solute redistribution within the profile; and
3. Examine how the hydraulic structure and physical properties (total and effective porosity, hydraulic conductivity, bulk density) within the peat profile control the rates and patterns of solute accumulation in unsaturated conditions.

3.2 Study Site

The study site (Exp Bog) is a 4 500 m^2 area (Figure 3-1) located in the James Bay Lowland, at the De Beers Group of Companies Victor Mine (51°51’13”N, 83°56’26” W, 85 m asl). It is on the margin of a domed bog, which gently slopes towards a stream, although the regional topography can be considered near flat. The site extent is defined by the final shape of a NaCl plume generated during a 45-day continuous solute release experiment, which is discussed in more detail in Chapter 2 of this thesis. There is a distinct hummock and hollow microtopography formed by the *Sphagnum* mosses. The hummocks are typically 0.5 to 1.0 m in diameter and 10-15 cm high. *Sphagnum fuscum* and *S. rubellum* form the hummocks while the hollows are

composed mainly of *S. majus*. Stunted 1-4 m *Picea mariana* (black spruce) trees are found scattered throughout the site, increasing in density towards the south. Peat thickness varies between 1.25 to 2.15 m. Average January and July temperatures (1981-2010 climate normals) are -20.7 and 15.4 ^{o}C at Moosonee (250 km southeast), and -22.4 and 17.1 ^{o}C at Lansdowne House (300 km southwest), and average annual precipitation is 700 mm and 681 mm, respectively, with 30% and 35% falling as snow, respectively (Environment Canada, 2015a, 2015b).

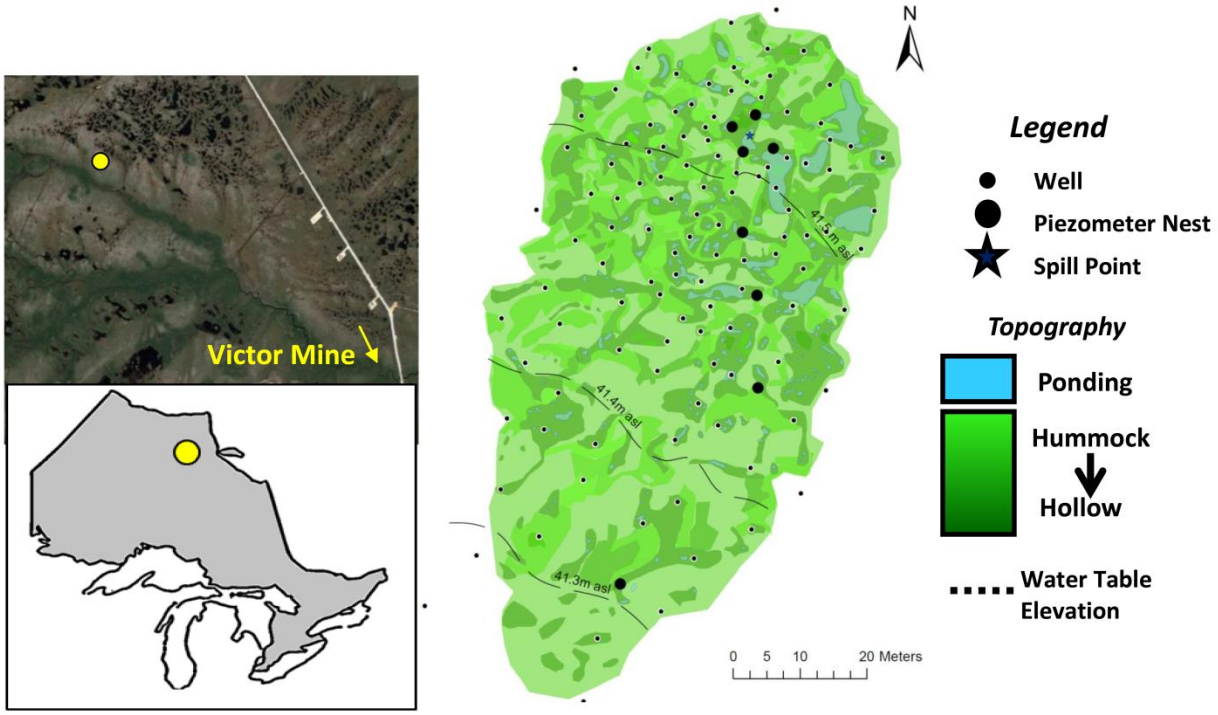

Figure 3-1 Location of the Experimental Bog (Exp Bog) in the James Bay Lowlands (bottom left) relative to the De Beers Group of Companies Victor Diamond Mine (top left). Site water table, microtopography and well and piezometer installations are also shown (right).

3.3 Methods

3.3.1 Field Experiment

Unsaturated zone field data were collected during a 45-day solute injection experiment conducted at the Exp Bog in 2015 between July 5 (day 0) and August 18 (day 45). Actual injection began at 17:00 h on day 0. Sodium chloride (NaCl) was used as the solute tracer due to its relatively non-reactive nature and its ease of in-field measurement through the surrogate measure of specific conductance (SC) (Hoag & Price, 1995). Simhayov (2017) found SC strongly correlated to the Cl^- distribution in peat following the release of NaCl. At the injection point, fresh water mixed with a concentrated solution of sodium chloride in an outflow weir. From here it flowed into a perforated 4" PVC well slotted to a depth of 1.5 meters below ground surface (m bgs). Over the 45-day period the average flow rate of diluted NaCl solution into the injection well was 13 500 L/day, with an average NaCl mass flux of 2.7 kg/day and average specific conductance of 543 µS/cm. A more detailed explanation of the injection system is described in Chapter 2 of this thesis.

To measure NaCl movement in the unsaturated zone, four hummocks (F1-F4) within 10 meters of the injection point were instrumented with three Campbell Scientific CS 615 probes connected to a Time Domain Reflectrometer (Campbell Scientific TDR 100) (Figure 3-2). Probes were installed 5, 10, and 15 cm bgs of each hummock. Bulk SC and dielectric constant data were recorded using these probes every 20 minutes on a Campbell Scientific CR1000 logger. Water content was determined given the K_a values using the method outlined in Kellner and Lundin (2001)

$$\theta = 3.9 * 10^{-2} + 3.17 * 10^{-2} * K_a - 4.5 * 10^{-4} * K_a^2 + 2.6 * 10^{-6} * K_a^3 \quad \textbf{Eq. 3-1}$$

where θ is the soil water content and K_a is the dielectric constant. Bulk SC values were corrected for water content to determine porewater SC using the method outlined in Hilhorst, 2000

$$SC_p = \frac{K_a{}'SC_b}{(K_a - 4.0)} \quad \textbf{Eq. 3-2}$$

where SC_p is the SC of the pore water (µS/cm), SC_b is the bulk SC (µS/cm), K_a is the dielectric constant measured by the TDR probe, and $K_a^{'}$is the real portion of the dielectric permittivity of the soil pore water (-) which can be determined using soil temperature

$$K_a{}' = 80.3 - 0.37 * (T - 20) \quad \textbf{Eq. 3-3}$$

where T is the soil temperature (°C), assumed equal to surface water temperature measured in wells.

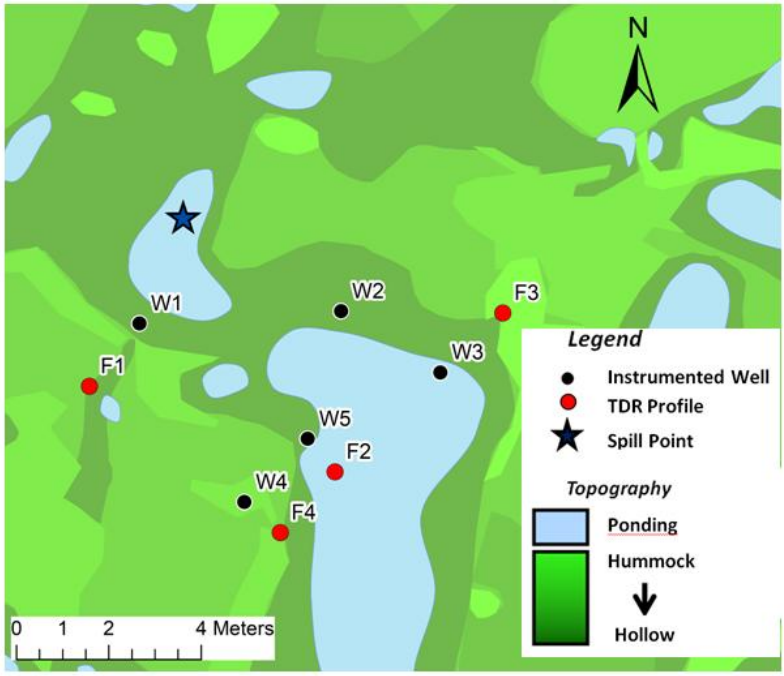

Figure 3-2 Location of the four TDR profiles (F1-F4 at 5, 10, 15 cm bgs) and the five wells (W1-W5) used for paired saturated/unsaturated zone analysis.

Saturated zone SC and water temperature data were collected from five 1" PVC wells (W1-W5 in Figure 3-2) that were slotted over a 1.25 m interval, screened with geotextile filter

sock (Rice Engineering & Operating LTD., 2" Filter Sock) and sealed at the bottom to prevent upwelling. Water temperature was recorded at 30-minute intervals using Schlumberger Mini-Diver D1501 pressure transducers installed in wells W1-W5. SC values were recorded in W1 and W3 at 30-minute intervals using Hobo fresh water conductivity data loggers. Manual measurements of water temperature and SC were also taken at wells W1-W5 and compared to logged results to ensure consistent logging accuracy.

Precipitation totals were averaged every 20 minutes using a tipping bucket rain gauge (Texas Instruments TE525M-L tipping bucket rain gauge) installed at the Exp Bog and recorded on a Campbell Scientific CR1000 data logger. Evaporative fluxes were determined using field data fitted using the Priestley-Taylor combination model. Details are provided in Chapter 2.

3.3.2 Unsaturated Solute Breakthrough Experiment

Four peat monoliths (L1-L4) were collected from hummocks directly north of the Exp Bog all within a 5 m radius, in 19 litre buckets, representing the upper 30 cm of the peat profile. The monoliths were frozen for preservation prior to shipment, and refrozen upon arrival at the lab to prevent decomposition. Each monolith was then shaved while frozen, to tightly fit into a 25 cm (inner diameter) polyvinyl chloride (PVC) conduit, sealed at the bottom to prevent leakage, but with a spigot for water supply. The monoliths comprised the undisturbed upper part of the peat profile including the living vegetation (visible non-moss vegetation was trimmed as part of core preparation). These mesocosms were used to test and simulate the rise of solutes into the unsaturated zone under controlled conditions.

For the duration of the experiment the four mesocosms were bolted to platforms in a climate controlled room. Relative humidity was maintained at 35% using a combined humidifier/ dehumidifier system. Relative humidity and temperature were measured using an RH probe and recorded using a Campbell Scientific CR1000 datalogger at 20-minute intervals. The bottom

outlet of each mesocosm was connected to a Marriot system to supply water for ET and to hold the water table in the mesocosm 5 cm above its bottom (Figure 3-3).

Each mesocosm was outfitted with Campbell Scientific CS 615 probes at 5, 10 and 15 cm bgs (measured from the top of each core) for the measurement of bulk SC and water content at five-minute intervals. Values of SC were corrected for water content using Equation 3-2.

Tensiometers composed of a porous clay cup and flexible silicon tube open to the atmosphere were installed at 5, 10, and 15 cm bgs for daily manual measurement of water pressure. Small pans of water were placed adjacent to the top of each core and weighed daily to determine difference in evaporative rates as a function of mesocosm placement in the room. Sampling ports were installed at 7.5, 12.5 and 17.5 cm bgs for the extraction of 5-10 mL of porewater for anion and cation analysis. Background sampling occurred one day before solute introduction and biweekly thereafter. Pore-water was extracted using 5 cm long porous ceramic sampling tubes (19.21.05, Rhizon, Rhizonsphere, Germany) connected to a syringe dedicated to each port, which collected a sample over a 12-hour period using consistently applied suction. Prior to sample collection each syringe was purged three times with ultra pure water. One duplicate sample was collected for every 10 samples collected. Anions were analyzed at the University of Waterloo Biogeochemistry laboratory using a Thermo Scientific Dionex Ion Chromatograph.

Figure 3-3 One of four cores used in the unsaturated solute breakthrough experiment. The bottom outlet of each core was connected to a Marriot system (far right) that maintained the water table 5 cm above the bottom. Three CS 615 probes (far left) and three tensiometers (right side of core) were installed at 5, 10 and 15 cm bgs to measure SC, water content, and water pressure. Three sampling ports were installed at 7.5, 12.5 and 17.5 cm bgs for biweekly sample extraction.

Prior to the start, each core was flushed slowly from the bottom with one pore volume of 300 mg/L sodium chloride solution, followed by a minimum of five pore volumes of ultra pure water (18.2 MΩ·cm). Ultra pure water was then added to each Marriot tube and the system was left for two months to minimize subsidence during the experiment period and to achieve steady-state evaporative conditions. At 12:00 h on day 0 of the solute breakthrough experiment a 300 mg/L solution was added to the Marriot system. The solute within the Marriot tube was continuously mixed using a timed low flow 12-volt mini water pump for five minutes every hour to prevent stratification. The experiment duration was 65 days from the time of initial NaCl addition. Water level in the Marriot system was measured daily with a measuring tape and refilled as necessary.

Post experiment, an ANOVA simple linear regression (95% confidence interval) was performed on the SC and Cl^- concentration values to determine the closeness of fit. The SC datasets, which had statistically significant correlations to Cl^- data were transformed using the equation of the fitted line. Chloride concentration values were also converted to mass within a sampling interval for better comparison of mass flux between cores using

$$M_{cl} = C_{cl} A_{core} h\theta \qquad \textbf{Eq. 3-4}$$

where M_{cl} is the chloride mass at a sampling interval, C_{cl} is the chloride concentration at that sampling interval, A_{core} is the cross-sectional area of the core, h is the height of the sampling interval (assumed to be 5 cm centered around each sampler) and θ is the volumetric water content.

3.3.3 Physical Soil Properties

After the end of the solute breakthrough experiment, each mesocosm was flushed repeatedly with ultra pure water until the outflow conductivity reached background values. Each mesocosm was then subdivided into two cores of 10 cm diameter, and then sliced into 5 cm vertical sections for soil property analysis.

Water retention and unsaturated hydraulic conductivity (K_{unsat}) were determined for each 5 cm slice at increasingly negative pressure steps (-5, -10, -15 and -25 cm) using the tension disk method outlined by Price *et al.* (2008). Hydraulic conductivity and core mass were measured for each pressure step and curves for K_{unsat} and volumetric water content (θ) were generated as a function of soil water pressure (ψ).

The saturated hydraulic conductivity (K_{sat}) was measured using a Darcy permeameter under steady state conditions. Each 5 cm section was sealed using a layer of plaster of paris followed by a layer of paraffin wax and inserted into a sealed rubber pipe connected to an outflow tube at the bottom. Water level above the slice in the sealed rubber pipe was maintained

at 5.5 cm above the outflow tube producing a hydraulic gradient of 0.85. Timed measurements of outflow were recorded until the flow rate reached equilibrium. Darcy's law was then used to calculate the resulting hydraulic conductivity

$$K = \frac{Q}{A}\frac{\Delta l}{\Delta h} \quad \textbf{Eq. 3-5}$$

where K (m/s) is the saturated hydraulic conductivity, Q (m^3/s) is the outflow, A (m^2) is the cross-sectional area of the slice, Δl (m) is the length of the slice, and Δh (m) is the difference in hydraulic head between the inflow and the outflow.

Effective porosity was determined using the method outlined by McCarter and Price (2017a); each 5 cm slice was saturated for 24 hours then placed in a pressure cell with a 1-bar pressure plate (Soil Moisture Equipment Corp. 5 Bar Pressure Plate Extractor) at -100 cm until water no longer drained from each slice. Each slice was reweighed after equilibrium was achieved. Effective porosity was calculated by assuming it was equal to the volumetric water content

$$n_e = \theta_{-100cm} = \frac{(M_{sat} - M_{100cm})}{V_t\,\rho_w} \quad \textbf{Eq. 3-6}$$

where n_e (-) is the effective porosity, M_{sat} (g) is the saturated mass of the slice, M_{-100cm} (g) is the mass of the slice at a drainage pressure of -100 cm, ρ_w (g/cm^3) is the density of water, and V (cm^3) is the volume of the section.

Sections were dried at 110 °C for 48 hours and weighed to determine the dry mass. Saturated and dry bulk densities were calculated by dividing the mass at each respective state by the section volume.

Total porosity was assumed to be the water content at 100% saturation. Volumetric water content was calculated for saturation and all pressure steps in the K_{unsat} experiment as

$$\theta_w = \frac{V_l}{V_t} = \frac{(M_\psi - M_{dry})}{V_t \rho_w} \quad \textbf{Eq. 3-7}$$

where M_ψ is the mass of the slice at the given pressure condition, M_{dry} is the mass of the dry slice, ρ_w is the density of water, and V_t is the measured sample volume.

3.4 Results

3.4.1 Field Experiment

The 2015 field season experienced a wetter summer than average, with a total of 233 mm of precipitation between July 5 and August 19 (Figure 3-4) compared to the July-August combined climate normal of 175 mm (1981-2010) (Environment Canada, 2015a; 2015b). The water table in the vicinity of the instrumented hummocks was within 5-20 cm of the surface (Figure 3-4). ET was relatively consistent compared to precipitation, with an average rate of 1.4 mm/day. The water table was at or above probe depth at 6 of 12 locations (F2-5 cm, F2-10 cm, F2- 15 cm, F3-15 cm, F1-10 cm and F1-15 cm); data from these locations were not used as they remained saturated.

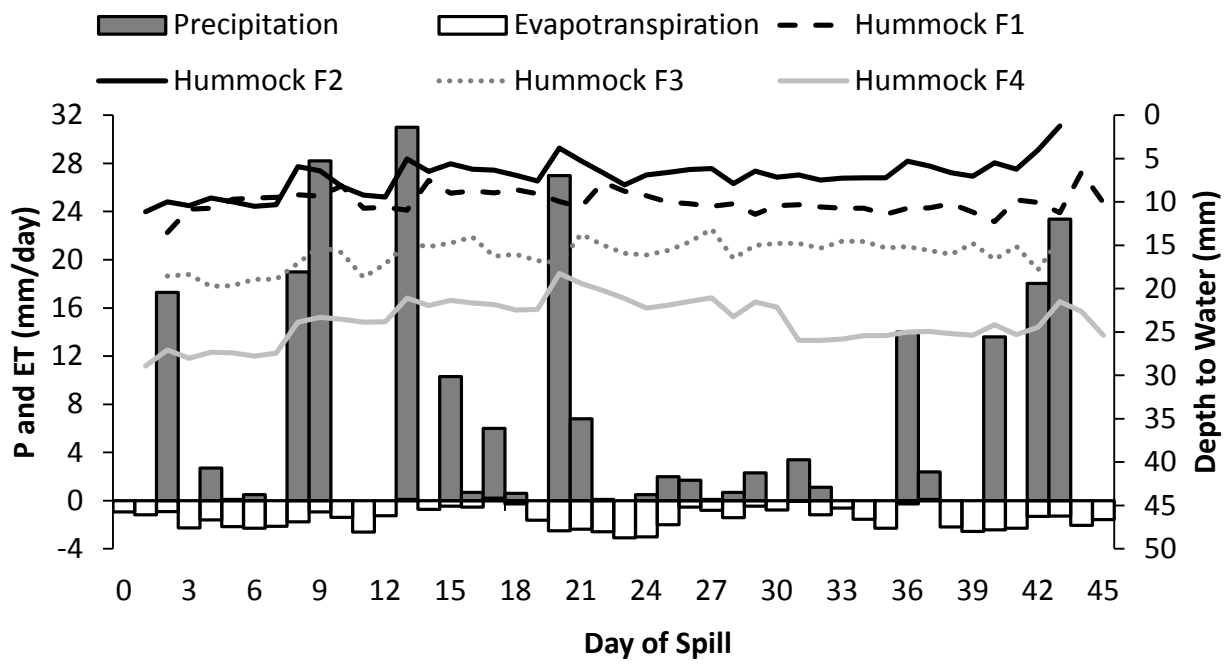

Figure 3-4 Daily precipitation and evapotranspiration (primary y axis), and depth to water table (secondary y axis) in the vicinity of the instrumented hummocks over the spill duration.

Saturated zone (well) SC values were comparable between locations, fluctuating with the major rainfall events on days 2, 8-9, 20-21, and 41 (Figure 3-5). Background unsaturated porewater SC values (initial values in Figure 3-5) varied by location (~200 µS/cm in Hummock F4, 200-400 µS/cm in Hummock F3, and 600 µS/cm in Hummock F1). Unsaturated zone response to saturated zone SC fluctuations varied between location and probe depth. In Hummock F4, porewater SC at the 15 cm probe (F4-15) followed a delayed and muted response to rainfall compared to the saturated zone until day 20. The day 20 rainfall event caused the highest response, increasing the SC by ~600 µS/cm. After this event porewater SC values declined steadily for the remainder of the spill. Porewater SC at the F4-10 and F4-5 probes did not increase until the day 20 rainfall event in which the SC values increased by 400 µS/cm and

200 µS/cm, respectively. The 10 cm probe SC then declined slightly over the remainder of the spill while the 5 cm probe SC remained elevated.

In Hummock F1, SC in the 5 cm probe (F1-5) responded minimally to saturated zone processes. The porewater SC at this depth only increased after the day 20 rainfall event, at which time porewater SC increased by ~200 µS/cm, remaining elevated for the remainder of the spill. At Hummock F3, probe F3-10 porewater SC responded in a similar manner to the F4-15 probe, with delayed and muted fluctuations compared to the saturated zone SC. The day 20 rainfall event resulted in the largest SC spike (~600 µS/cm) after which the porewater SC slowly declined for the remainder of the spill period. Probe F3-5 porewater remained unchanged until the day 20 rainfall event, after which it increased by 400 µS/cm before maintaining a peaked porewater SC for the remainder of the spill.

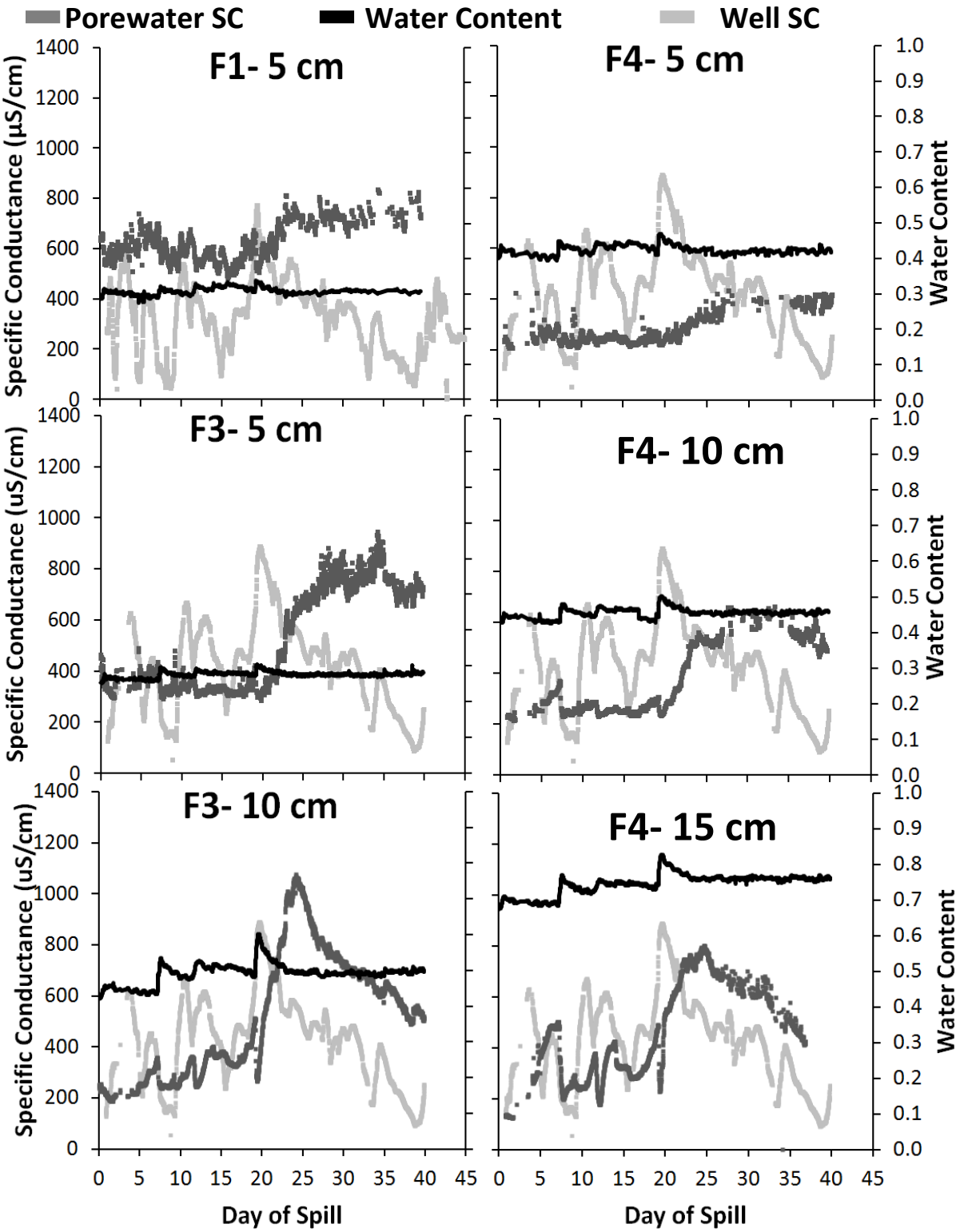

Figure 3-5 Pore water SC for selected TDR probes (dark grey) and corresponding water content (black). Also shown is the paired well SC (light grey) representing the saturated zone.

3.4.2 Unsaturated Solute Breakthrough Experiment

Over the 65-day solute breakthrough experiment, relative humidity (34±3%) and air temperature (26.5±1.7 °C) remained stable. Evaporation rates from water pans placed at each of the four cores showed little spatial variance (Figure 3-6); the cumulative difference between Pan L1 which experienced the most evaporation and Pan L4 which experienced the lowest evaporation was 14 mm.

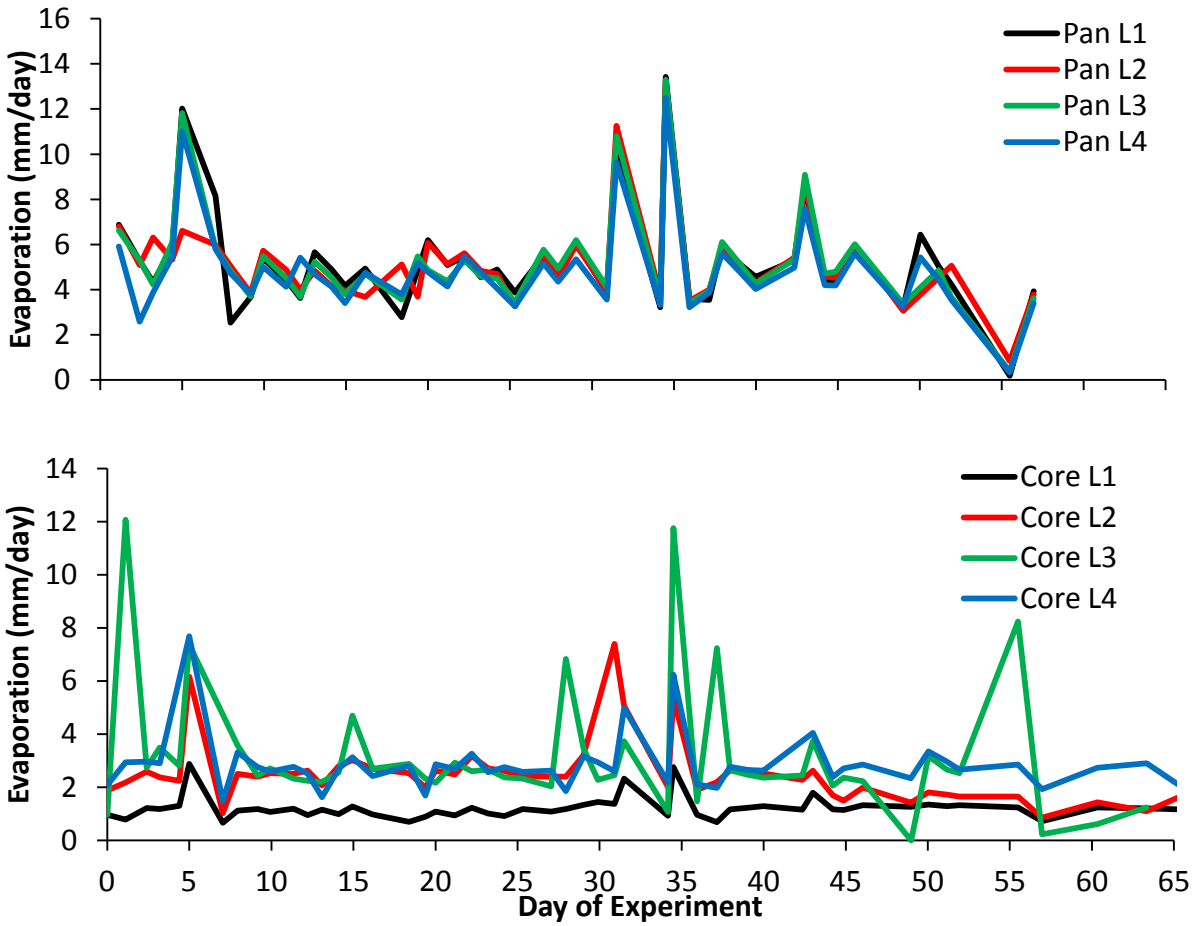

Figure 3-6 Daily evaporative rates of open water at each core (top), and daily evaporative rates from each peat core (bottom).

Daily rates of evaporation differed between cores, with a total evaporative depth of 64, 127, 157, and 144 mm in cores L1, L2, L3 and L4, respectively, over the 65-day period. Total solute addition to each core, determined by multiplying the volume of water cumulatively added

to each Marriot system by the concentration of NaCl in solution, consequently varied by core. Core L3 received a total of 1.3 kg of NaCl while Cores L2 and L1 only received 0.95 kg and 0.58 kg, respectively. Core L4 was used as a control for background conditions and thus did not receive NaCl.

Water content, pressure head, chloride concentration and SC data are shown for the 5 cm, 10 cm and 15 cm depths for each core on Figures 3-7 through 3-10. For all cores which underwent solute addition (F1-F3) there was a statistically significant correlation between the SC and Cl^- datasets, and all R^2 values were greater than 0.9 (Figures 3-7 to 3-10). The fitted lines (Appendix Figure A-2) were used to transform the SC dataset to the Cl^- concentrations shown on the Figures. Chloride mass calculated at each sample interval is also shown on Figures 3-7 to 3-10. In all columns, with the exception of L2-5 due to a seal break, ψ declined over the experiment, signalling hydrological non-steady state conditions. Vertical hydraulic gradients for each core are shown in Figure 3-11.

The average chloride concentration in Core L4 (no solute added) was 0.55 mg/L and did not increase with depth or elapsed time over the experiment (Figure 3-7). Soil-water pressure remained highest at L4-15 and lowest at L4-5, creating an upwards vertical flow gradient that remained constant despite the changing water contents and pressures over time (Figure 3-11).

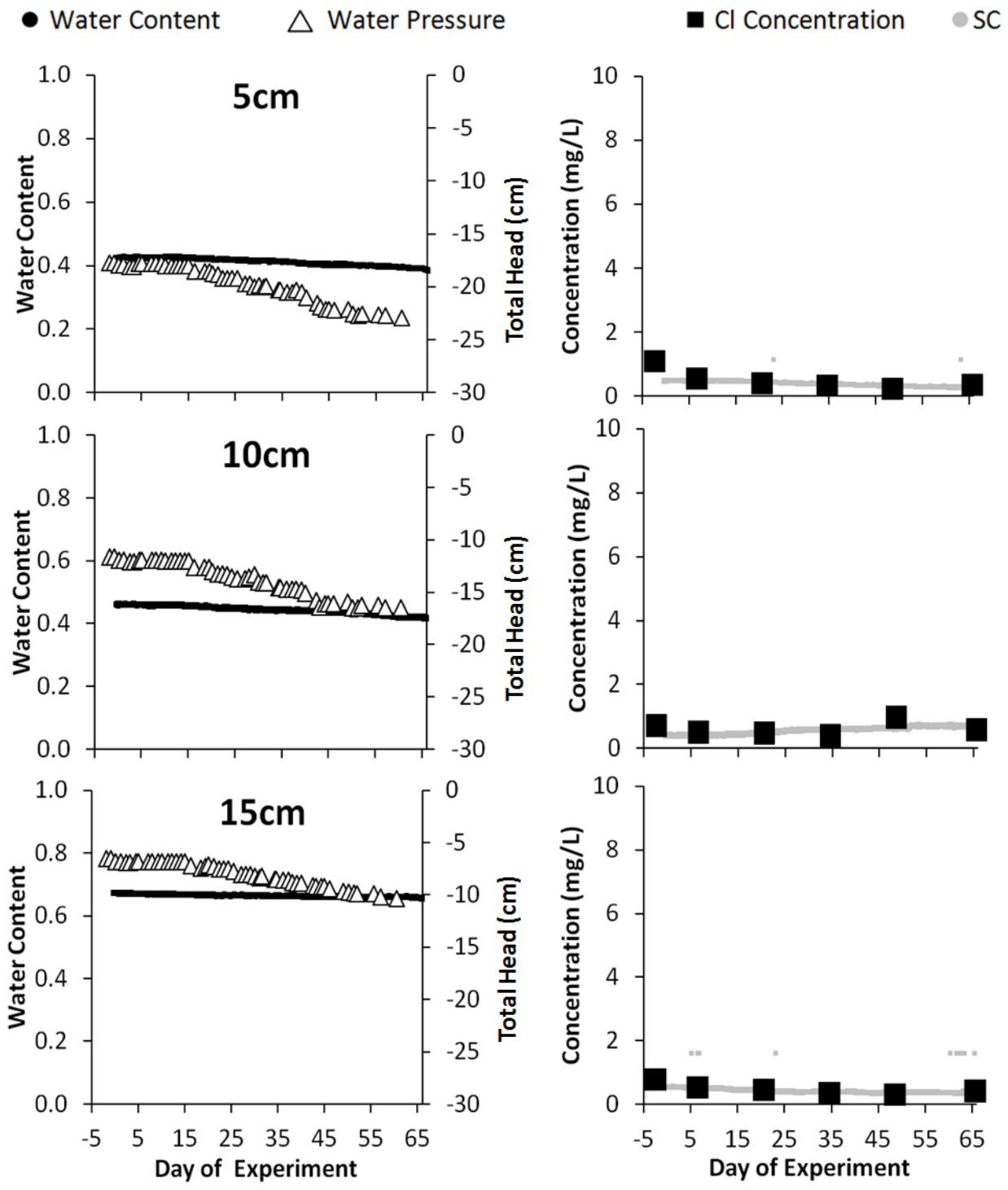

Figure 3-7 Core L4 water content and water pressure (left) and Cl^- concentration with fitted SC using a simple linear regression (right) at 5, 10, and 15 cm depths.

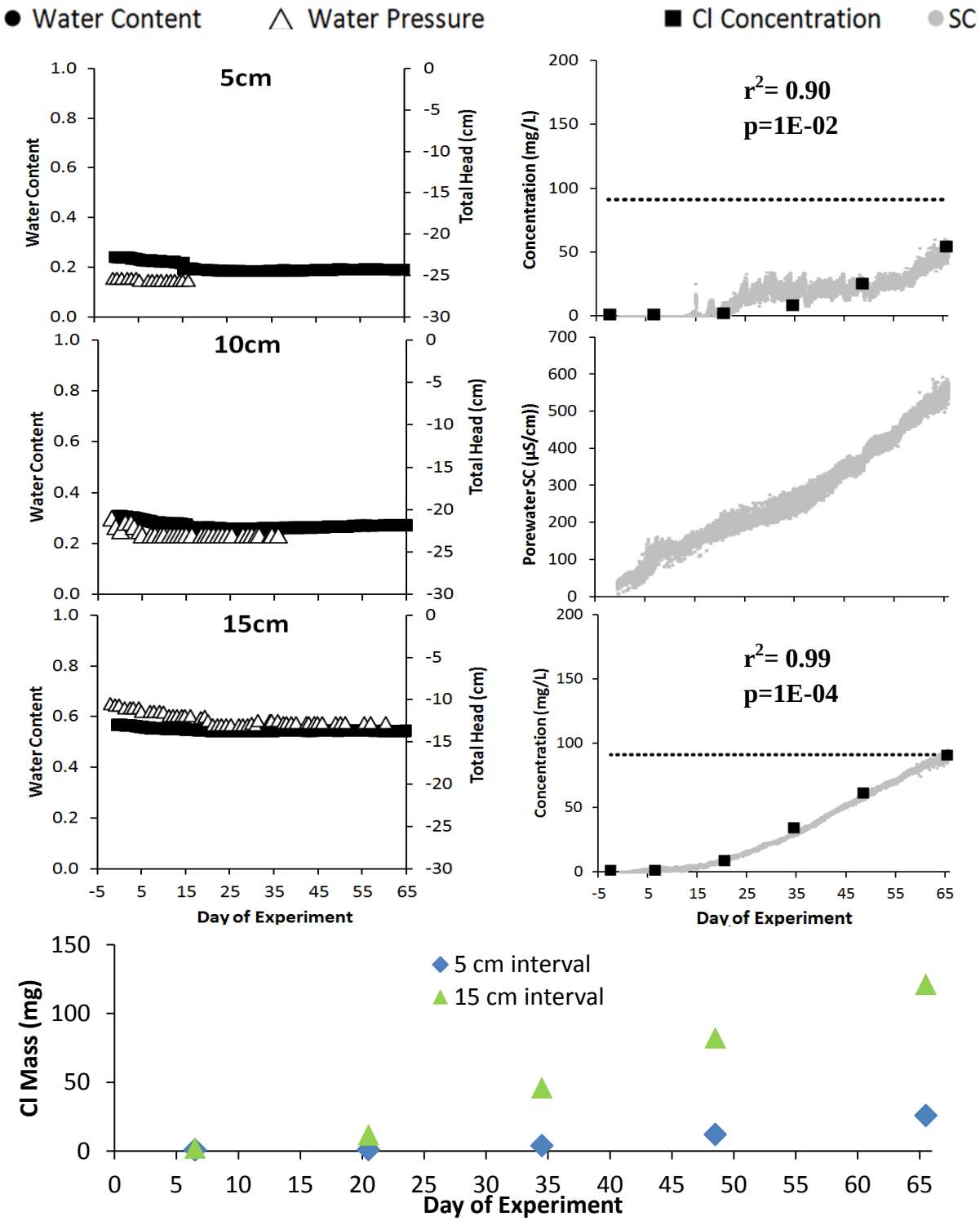

Figure 3-8 Core L1 water content and water pressure (top left) and Cl⁻ concentration along with fitted SC using a simple linear regression (top right) at 5, 10, and 15 cm depths below core surface. Dashed lines represent the 50% breakthrough concentration for chloride. Due to an inability to extract samples chloride regression is not shown at the 10 cm depth. Also included is the cumulative Cl⁻ mass at each depth (bottom).

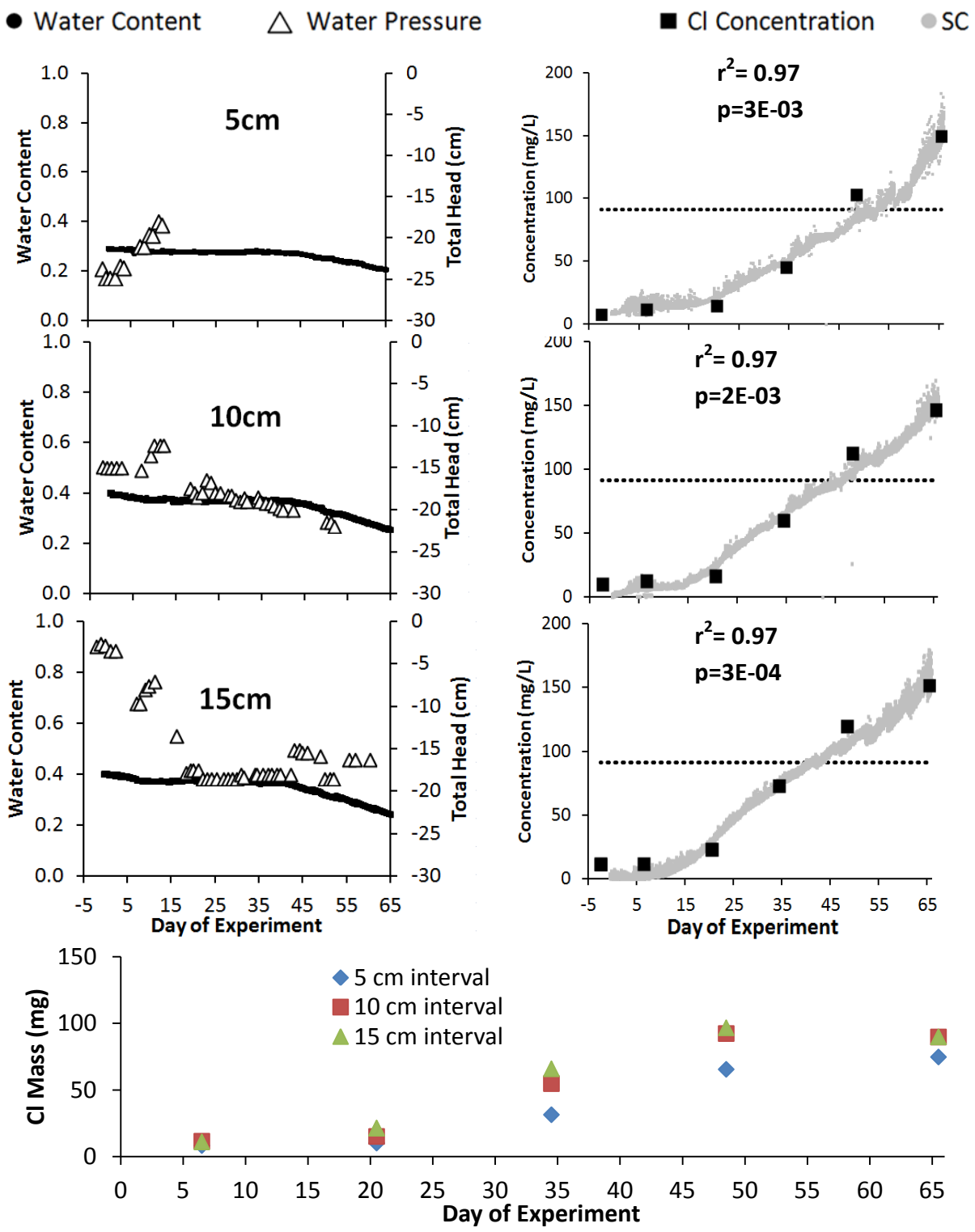

Figure 3-9 Core L2 water content and water pressure (top left) and Cl⁻ concentration along with fitted SC using a simple linear regression (top right) at 5, 10 and 15 cm depths below core surface. Also included is the cumulative Cl- mass at each depth (bottom).

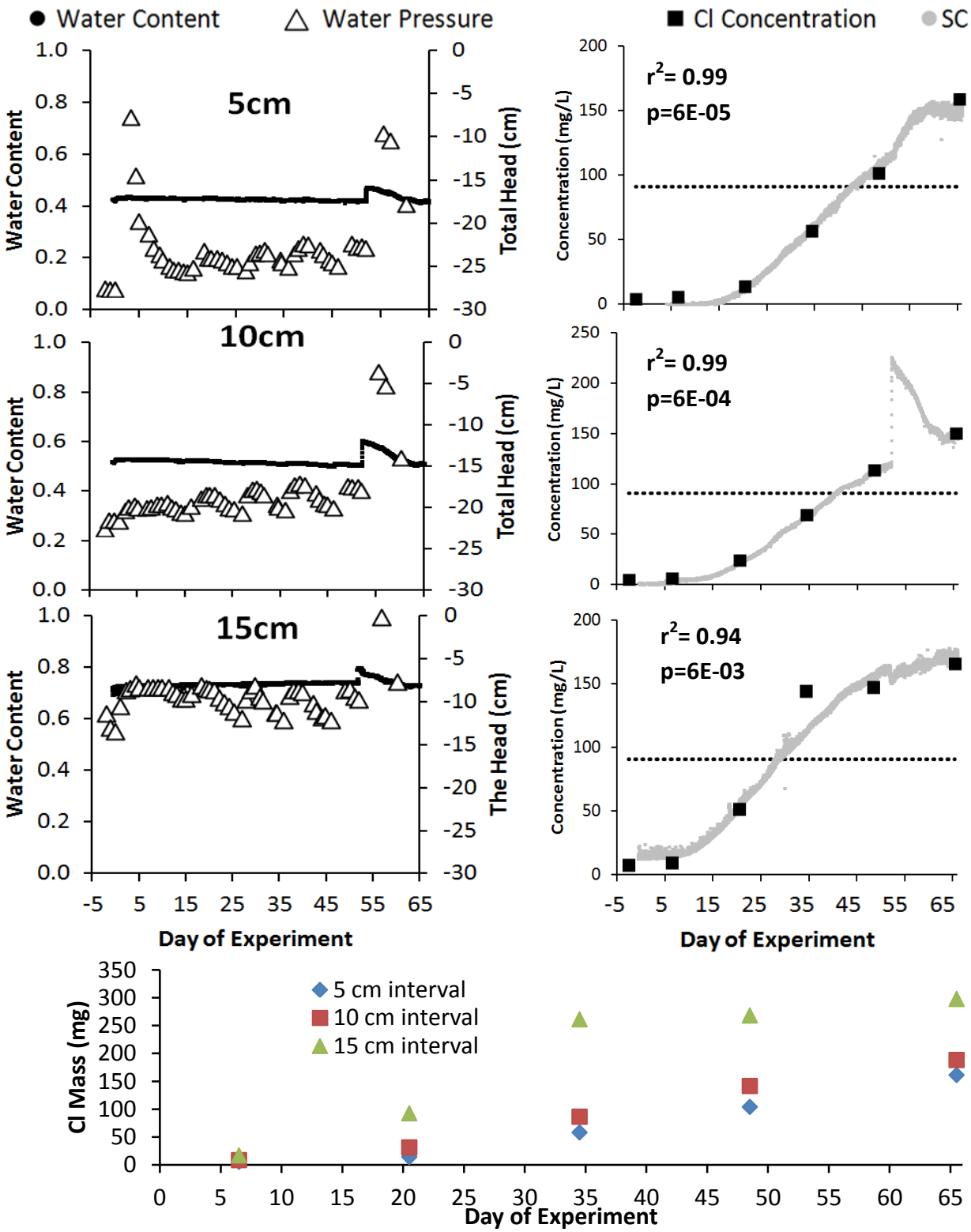

Figure 3-10 Core L3 water content and water pressure (top left) and Cl^- concentration along with fitted SC using a simple linear regression (top right) at 5, 10 and 15cm depths below core surface. Also included is the cumulative Cl^- mass at each depth (bottom).

In Core L1 (Figure 3-8), chloride concentrations at all three measurement depths did not increase noticeably until day 15, in which a small decrease in volumetric water content was also observed at all three depths. By day 25 the chloride concentration plateaued at L1-5 until day 55, however Cl^- continued to increase linearly at L1-10 and L1-15. The 50% breakthrough of chloride concentration occurred at L1-15 at day 65, but did not occur at L1-5 during the experiment period. Due to the inability to collect samples at the L1-10, and the inconsistency of SC-Cl relationships between probes, it is unknown whether or not breakthrough occurred in this layer. Chloride mass movement mimicked that of concentration (Figure 3-8); a greater portion of mass remained at the 15 cm interval than the 5 cm interval. Vertical pressure gradients appeared constant until suction was lost (instrument failure) by day 30 (Figure 3-11). The average upwards gradient was much lower at the 10/5 cm interval (0.55) compared to that at the 15/10 interval (2.16).

Chloride concentrations in core L2 (Figure 3-9) did not notably increase until on, or shortly before, day 15 after which they increased linearly at all three measurement depths. The 50% breakthrough of concentration occurred on day 40 at L2-15, day 44 at L2-10, and on day 50 at L2-5. Interestingly, solute mass tells a different story. By day 65 chloride mass appears to be equivalent at all depths, and did not increase between days 50 and 65 (Figure 3-9 bottom). In Core L2 gradients at both depth intervals decreased rapidly after the start of the experiment, losing suction at the 10/5 cm interval and dipping below zero at the 15/ 10 cm interval between days 5 and 25. No evidence of suction loss (i.e., air entry at the tube/core interface) was observed between the 15/ 10 cm interval, suggesting the gradient was not due to instrument failure.

Chloride concentrations in L3 (Figure 3-10) remained at background values at all depths until days 10-15, after which concentrations increased linearly until the day 50 seal break

(instrument failure). The 50% breakthrough occurred at day 28 at L3-15, day 40 at L3-10 and day 42 at L3-5. Chloride mass movement mimicked that of concentration (Figure 3-10 bottom). Internal vertical pressure gradients remained constant after day 7 at the 10/5 cm interval, with an average of 1.41. On day 50 the 15/10 cm gradient decreased rapidly due to the Marriot tube seal break (instrument failure) on this day.

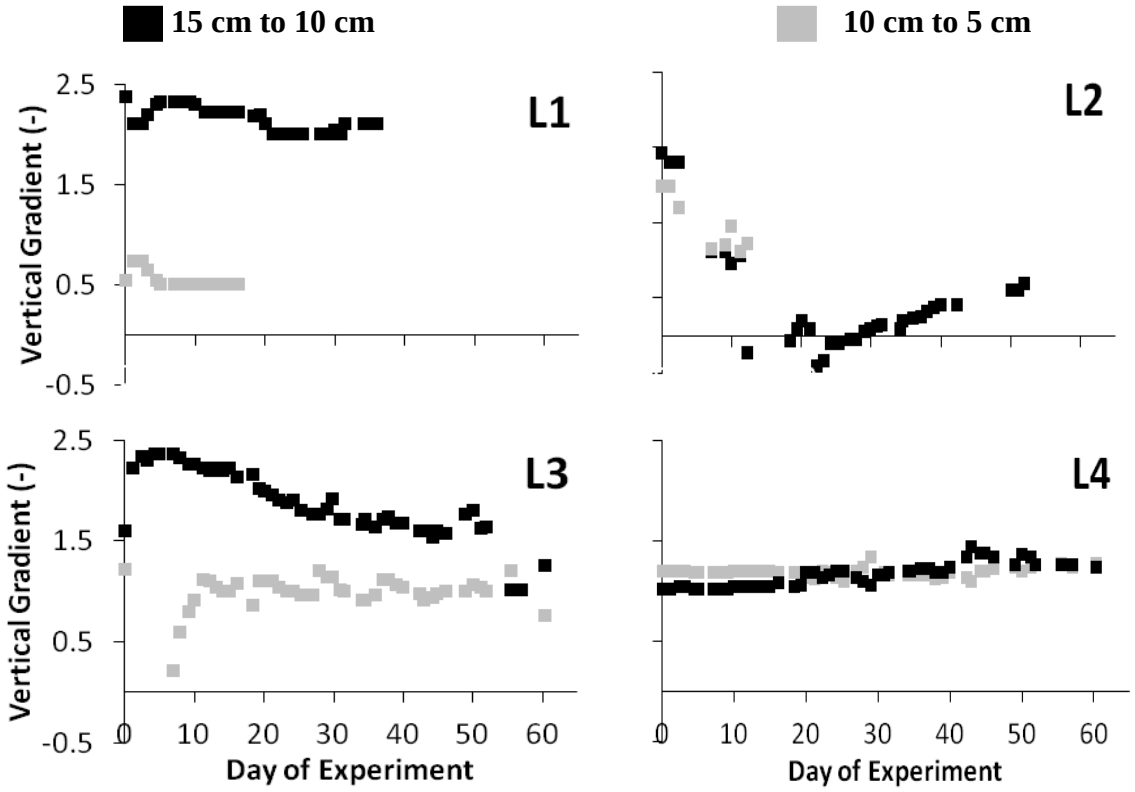

Figure 3-11 Vertical gradients between the 15-10 cm and 10-5 cm depths for each core, calculated by subtracting the difference in soil water pressure and dividing by vertical distance (5 cm).

3.4.3 Physical Soil Properties

The four cores displayed the same general trend of increasing dry bulk density, and decreasing total porosity with depth in the first 20 cm bgs (Figure 3-12); thereafter the trend gently reversed or was stable with greater depth. Effective porosity increased in Cores L1 and L4 and decreased in Cores L2 and L3 between the 0-5 and 5-10 cm slices. Effective porosity

decreased in all cores between 10 cm bgs and 20 cm bgs. Below the 20 cm depth, each core experienced a small decrease in bulk density and small increases in both total porosity and effective porosity. Variability in these parameters between each core was the highest in the top 15 cm bgs.

Depth profile data from the saturated and unsaturated water retention and hydraulic conductivity experiments are summarized in Figure 3-13. For all cores the top ten centimeters had the lowest bulk density and the highest total and effective porosity. The saturated volumetric water content and K_{sat} were also highest in this interval; however at pressures < 0 cm the water content became the lowest at this interval for all cores and the K_{unsat} dropped to within measurement error of the lower depths. Unsaturated hydraulic conductivity values decreased by 3 orders of magnitude between 0 and -5 cm soil water pressure for all depths and all cores, resulting in K_{unsat} values ranging between 5×10^{-7} and 5×10^{-8} m/s at lower soil water pressures.

Below 10 cm behaviour varied by core, however slices with a higher bulk density had lower effective porosity, θ_{sat} and K_{sat} but higher θ at pressures < 0 cm and a slower decline in K_{unsat} at increasingly negative pressures.

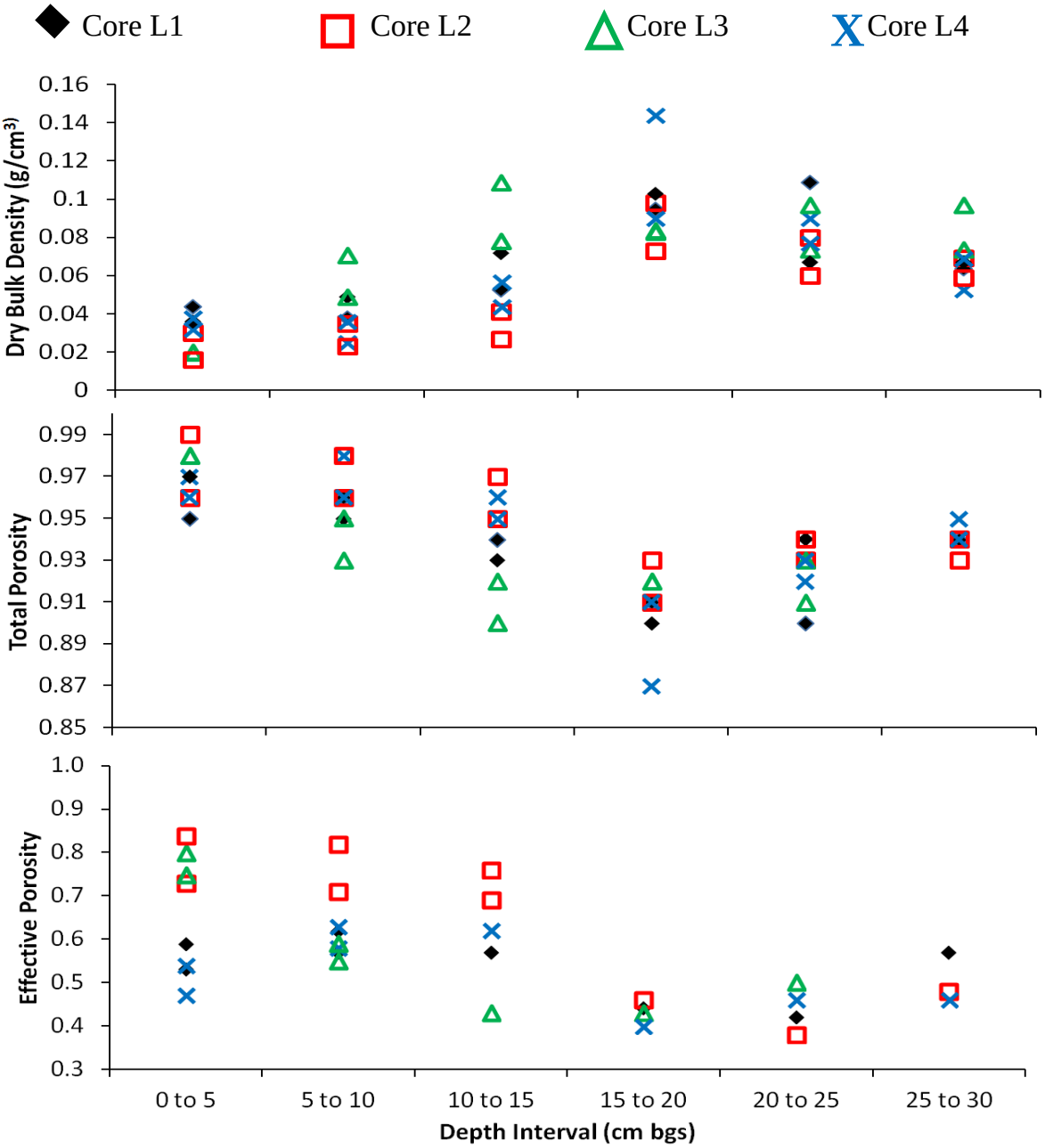

Figure 3-12 Soil dry bulk density (top), total porosity (middle) and effective porosity (bottom) measurements for Cores L1-L4 taken from 5 cm slice data in duplicate.

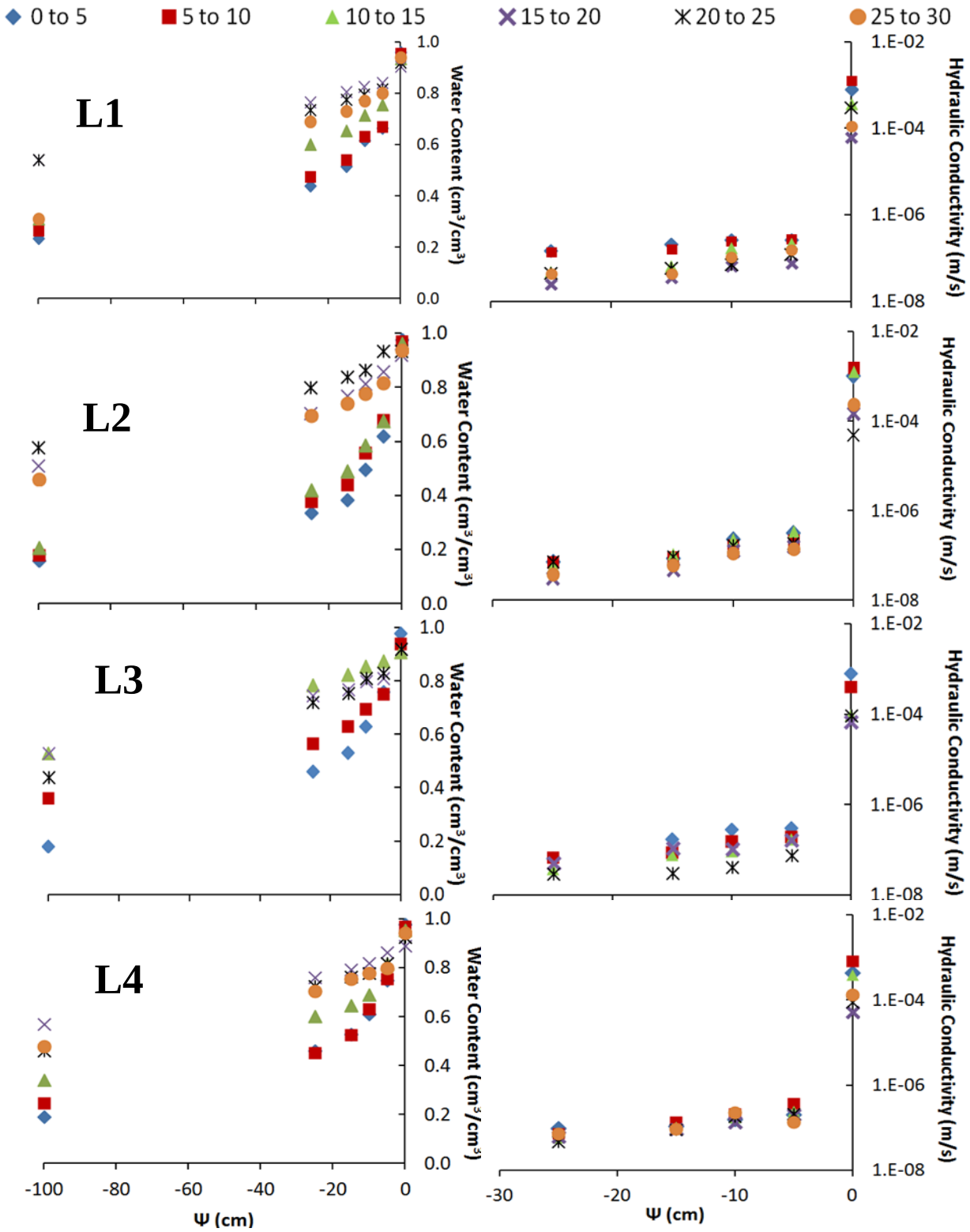

Figure 3-13 Volumetric water content (left) and vertical hydraulic conductivity (right) for cores L1-4 (top to bottom) as a function of negative soil pressure, or distance above the water table.

3.5 Discussion

3.5.1 Field Experiment

Despite being within a 5 m radius, Hummocks (F1-F4) experienced variable hydrological and contaminant transport behaviour. In the saturated zone, well SC spikes (Figure 3-5) occurred directly after the large rainfall events on days 2, 8-9, 13, 19-20, and 40, simultaneous with an increase in water table elevation (Figure 3-4). This is contrary to what may be expected given the dilution caused by rainfall. It suggests that there was an increase of solute movement from the nearby (<10 m) source directly after these rainfall events, due to increased saturation and flow in the highly permeable near-surface peat (Baird, 1997; McCarter & Price, 2017a, 2017b). This behaviour may also have been amplified by sampling from a well; samples drawn during periods of lower water table draw preferentially from lower, less contaminated layers. The water table peaks associated with rain events receded within a day or two of the event, although there was a general increase in water table up until the day 20 event, after which it remained relatively constant.

The water contents (θ) at the "saturated" probes; Hummock F1-10 cm (F1-10), F1-15, F2-5, F2-10, F2-15, and F3-15 (not shown) were within the expected range of total porosity (0.85 to 0.99) for the respective depths, reflecting their position at or below the water table. Probes F1-5, F3-10 and F4-15 were 5-8 cm above the mean water table, F3-5 and F4-10 were 11-13 cm above the mean water table, and F4-5 was 18 cm above the mean water table. In near-watertable (<5 cm) probes (F3-10 and F4-15), water contents fluctuated distinctly after each rainfall event up until day 20, after which they remained relatively constant (similar to the water table, which became high and relatively stable at this time). The enhanced fluctuations reflect the rise and fall of the water table or the capillary fringe, and storage of percolating water near the bottom of the profile. At these locations there was a delayed response of the porewater SC spike

compared to that in the saturated zone (Well SC) that is likely due to the time required for capillary rise to draw the elevated SC water upwards from the saturated zone. After each rainfall event, flushing was observed in the probes, as illustrated by the noticeable decrease in porewater SC.

The two probes which were located at depths 5-10 cm above the water table (F3-5 and F4-10), maintained a lower and more consistent water content. This is due to their greater distance above the water table and poorer water retention capacity of mosses higher in the profile (Figure 3-13). This typically results in a less responsive soil moisture regime (Price & Ketcheson, 2009) compared to the deeper peat (Figure 3-5). Porewater SC in both probes did not increase until the day 20 rainfall event, and the well-drained mosses, coupled with a low hydraulic conductivity, were unable to draw contaminated water to this level by capillary rise. By day 20, when the water table reached its high and consistent level, the distance to contaminant and capillary resistance were both minimized (5, 15 and 20 cm bgs, in F1, 3 and 4 respectively); consequently contaminated water arrived, and SC peaked. This behaviour is noted to an even greater extent in F4-5 (18 cm above the water table), in which there was a relatively small, and delayed arrival of solute-enriched water from below.

While proximity to the water table is important in determining water content at a given position in the peat profile, the very poor water retention capacity of the uppermost layers (Figure 3-13) renders them least sensitive to water table effects. Despite being 5 cm above the water table on average, probe F1-5 experienced water content similar to probe F4-5, which was 18 cm above the water table, on average, due to the poor water retention in both. Nevertheless, being only ~5 cm from the water table, F1-5 was closer to the solute source in the saturated zone, and its much higher SC than at F4-5 attests to its capillary rise to this level in the profile. The

maintenance of elevated SC at this depth suggests that the dead-end and closed pores, which remain saturated, may cause solute to partition into the inactive spaces and be held above the water table.

3.5.2 Unsaturated Solute Breakthrough Experiment

Prior to the execution of the laboratory experiment, care was taken to extract in situ hummock mesocosms that were as structurally similar to one another as possible. Additionally, care was taken to ensure that the ambient conditions in the laboratory chamber (i.e. temperature, humidity, and air flow) were maintained uniform and equally distributed. In spite of this, the soil physical properties determined in-lab showed a high degree of variability between cores, as did the rates of evaporation and vertical solute transport within them. The variability in soil physical properties reflects the high spatial variability in natural systems (McCarter & Price, 2014), even for samples selected for their apparent similarity. Despite a high degree of variability, soil parameters fell within expected ranges, including bulk density (Boelter, 1969; Carey *et al.*, 2007), total porosity (Boelter, 1969; Carey *et al*., 2007; Rezanezhad *et al*., 2010), effective porosity (Carey *et al*., 2007; Rezanezhad *et al.*, 2010), and water content/ K_{unsat} versus pressure relationships (Carey *et al.*, 2007; Gnatowski *et al*., 2010; Price & Whittington, 2010; Rezanezhad *et al.*, 2010). The pattern of decreasing bulk density/ increasing total and effective porosity noted at all four cores below the 15 cm depth was unexpected, however, and may be attributable to the presence of other vegetation. The unique hydrological and solute transport observations for each mesocosm reflects their differences in hydraulic and physical character. The potential for non-uniform conditions within the chamber to explain the differences is negated by the similarity of open water evaporation at each location (Figure 3-6).

During the experiment all four mesocosms experienced a net decrease in water content and pore water pressure over time for all depths (with the exception of Core L3 following the

failure of its Marriot system on Day 50). This is likely due to the extended time it takes for a large, relatively wet sample to come to equilibrium, as is reflected in the slow rate of change in the tails of the drainage curves (Figure 3-13).

For all cores that underwent NaCl additions, the SC data were highly correlated to the Cl^- concentrations (all fitted relationships statistically significant and $R^2>0.9$). This is consistent with behaviour observed by Simhayov (2017), where SC curves closely matched Cl^- movement, while deviating from that of Na^+ in both saturated and unsaturated breakthrough experiments. Na^+ retardation is caused by adsorption of Na^+ onto the peat surface, changing its pore-water concentration (Rezanezhad *et al.*, 2012).

Core L1 exhibited both the lowest rate of evaporation (average of 1.2 mm/day), and the least amount of upward solute transport, particularly evident in the upper 5 cm (Figure 3-8). There are no obvious trends in bulk density that explain this. However, the water retention capacity of L1 peat in the top 20 cm of the profile is uniformly low at the -100 cm soil-water pressure level (Figure 3-13). In other cores the water retention at -100 cm increases with depth, suggesting water is more likely to be retained higher in the profile than at L1, hence able to deliver water to the surface to sustain evaporation. The low evaporation at L1 is consistent with the low water content near the surface (see 5 and 10 cm values in Figure 3-8), which reduces K_{unsat} (Figure 3-13), restricting upward water movement. Furthermore, the hydraulic gradient between the 5 and 10 cm layer in Core L1 is very small (0.50), reflecting the nearly equivalent water contents and soil properties (bulk density and total/ effective porosity) at these depths. The low evaporation from L1 provides it with the least draw for solutes, and thus the least solute mass of all cores occurred at the L1-5 cm layer.

Core L2 experienced an average rate of evaporation of (2.5 mm/day) and 50% breakthrough at all three depths by day 50 of the experiment period (Figure 3-9). The Cl^- concentrations at each level are quite similar; however, when these values are translated into Cl^- mass (Figure 3-9 bottom) it is clear that Cl^- mass was consistently lower in the 5 cm interval, which is expected given a solute source at the bottom of the core. However, the 10 and 15 cm intervals had similar Cl^- masses after day 35, which leveled off between days 48 and 70. The decrease in water content during this period elevates chloride concentration without an actual increase in solute mass.

Core L3 experienced the highest rate of evaporation (3.4 mm/day) and 50% breakthrough at all depths by day 42 (Figure 3-10). Of note, 50% breakthrough occurred at the 5 cm layer in only 29 days, which was 14 days faster than Core L2. The physical structure of the top 15 cm of Core L3 appears to have created the most "ideal" conditions of the three cores for evaporation. The most distinctive difference is in the 10-15 and 15-20 cm layers, where Core L3 has distinctly higher bulk density than the other cores. Curiously, these layers in L3 have the lowest water retention compared to the other cores (e.g., at ψ = -20 cm), which should result in a lower effective K_{unsat}. However, it also has the least difference in water retention (thus K_{unsat}) between these two layers compared to the other cores at this depth, as well as the highest and most constant upwards hydraulic gradients of the cores that underwent solute additions. It is evident that small differences in hydraulic properties within a layer or between layers, can have a considerable effect on evaporation, thus capillary rise of solute. This needs to be investigated further by performing a sensitivity analysis using a 1-dimensional approximation of the Richard's equation, such as with Hydrus 1D (e.g. McCarter & Price, 2014).

Although not directly observed, the long term process of evapo-concentration would likely become important, particularly in the upper 5 cm of the cores. This behaviour was recorded in the unsaturated column experiment by Simhayov (2017), where surficial Cl^- concentrations were greater than input concentrations by day 120, where the water table was held 23 cm below the surface. It is likely that similar behaviour would have been observed if this experiment had been run for a greater time period, particularly in Core L3 where the rate of evaporation was particularly high.

Although not directly observed, it is likely that dispersion and diffusion into inactive pore spaces is influential in Cl^- and Na^+ mobility. Due to a lack of variability in water content, the dispersion was determined to be relatively uninfluential in unsaturated solute breakthrough modelling (Simhayov, 2017). There would be value in reassessing the sensitivity of an unsaturated HYDRUS model to dispersion in systems such as this, which operate for long periods of time at non-equilibrium conditions.

3.5.3 Relations Between Field and Laboratory Results

Relationships obtained through the controlled conditions and detailed analysis of the laboratory experiment can be used as a point of comparison with field values. In both the field environment and in laboratory mesocosms, the high variability of hydraulic and physical properties within and between peat profiles resulted in distinctly different solute transport and distribution behaviours. This highlights the importance of recognizing and accounting for significant heterogeneity when attempting to quantify processes using a finite number of samples (Goetz & Price, 2015; McCarter & Price, 2014). Under field conditions, the antecedent state and ongoing climatic events further influence the upward mobility and retention of solute.

In both laboratory and field experiments, the presence of well-drained peat near the surface limited upwards solute mobility. The very low water retention capacity of the uppermost

layer renders it somewhat independent of distance to water table, as evidenced by the similar behaviour of θ in Hummock F2-5 (5 cm above the average water table) and F4-5 (18 cm above the water table). However, the structure of the peat profile must be considered, since low water contents and low evaporation losses can result from surficial peat that is loose with an open pore structure, and especially when underlain peat of a similar structure. The optimal conditions for evaporation loss and solute rise is when the surficial peat is underlain by peat of decreasing porosity and increasing bulk density with depth (e.g. Core L3). This retains moisture higher in the profile and improves connectivity (higher K_{unsat}), both of which facilitates evaporation and consequently, solute rise.

3.5.4 Sources of Error

Despite the precautions taken to ensure undisturbed extraction and shipping of peat cores, it is likely that some loss of original structure occurred in the transportation process. Further, prior to the start of the experiment each core experienced additional subsidence in the amount of 5-7 cm during the 2-month settling period, suggesting an additional breakdown of original pore structure. This would be problematic if parameters derived from these cores were being used to drive simulations of field conditions, but this was not done here. All measured soil parameters were extremely sensitive to small changes in slice structure and weight, due to the small size of soil samples being tested.

3.6 Conclusions

Characterization of unsaturated zone solute behaviour faces a number of unique challenges at both field and laboratory scales. At field scale, saturated zone processes and hydrological conditions have a strong influence on the presence and amount of solute above the water table. Rainfall events, and a subsequent rise in water table elevation, increased connectivity between unsaturated hummocks and the saturated zone. In both laboratory and field

conditions, hummock structure and water content influence upwards solute transport to a great extent; loose (less dense) soil transmits solute well under saturated conditions, but drains quickly, which reduces the moisture content, hence in effective K_{unsat}. In denser soil, solute moves at a slower pace in saturated conditions, but since it retains more water, its effective K_{unsat} is higher and is better able to facilitate capillary rise and draw solute from the water table.

In controlled laboratory conditions, inter core heterogeneity results in highly varied hydrological and solute behaviour. The 50% breakthrough of Cl^- occurred at all depths in 2 of 3 cores in an unsaturated breakthrough experiment. Cores that experienced breakthrough had higher rates of evaporation and thus solute uplift. Highest evaporative and upward solute flux was seen in the core with a highly porous upper five 5 cm directly underlain by much denser, less porous peat, which could supply solute and increase the water content above it.

Measured core physical parameters fell within ranges specified by previous studies; however, a previously unreported decrease in bulk density and increase in total and effective porosity was noted in depths below 15 cm for all cores. Visual observation of the cores noted intact roots from vascular vegetation at this depth interval.

The long-term effect of evapo-concentration was not observed during the field experiment due to wet conditions, or in the laboratory experiment due to the limited time of the experiment (65 days). It is likely that under drier conditions and longer time scales evapo-concentration would play a more significant role in solute transport. However, given the 65-day experiment with zero recharge and flushing from above, it seems likely that rain events in a field setting could limit the accumulation of solutes in the top part of the profile.

Conclusions from this research may be used in the future to aid in soil parameterization in unsaturated zone solute transport modelling. Observed increases in porosity and decreases in

bulk density below 15 cm draws attention to potential error in assuming linear or exponentially increasing patterns with depth. Further, care should be taken when assuming extracted cores are representative of site conditions, as even cores taken within visually similar areas had markedly different solute transport behaviours both in laboratory and field conditions.

4 Conclusions and Recommendations

This study has identified key mechanisms which influence the fate and transport of a conservative solute in bog peat, both regarding saturated and unsaturated zone processes. Although conclusions from this study provide a solid foundation, they are representative of relatively short term conditions present during a solute release, which may not necessarily act as key drivers of long term behaviour. Further, the addition of contaminant specific behaviours such as sorption and biodegradation would likely increase the complexity of solute behaviour.

In the saturated zone, the high elevation of the water table facilitated lateral advection within the highly conductive acrotelm, particularly within the interconnected hollows in the landscape. The direction of solute advection was down the slope of the water table, even though it was slight (0.004 m/m). Advection was also enhanced over the first 24 hours by hydrological forcing of water, which resulted in groundwater mounding around the injection well. A second layer of plume advection was noted in a discontinuous high conductivity layer at ~125 cm bgs, corresponding to visual observations of relatively undecomposed woody material at this depth. This layer was likely "activated" due to the subsurface nature of the solute injection. Numerous rainfall events diluted the solute concentration in the upper, most hydrological active zone and temporarily masked the presence of the plume. Diffusion likely transported the solute into disconnected pore spaces and low hydraulic conductivity hummocks, as shown by lower but more stable SC values in hummocks than nearby hollows.

Vadose zone solute transport was largely influenced by below-water table conditions. Fluctuations in water table level influenced the connectivity of unsaturated hummocks and the saturated zone. Loose surficial peat has a high saturated hydraulic conductivity but low water retention capacity due to the large average pore size. In unsaturated conditions the water content

of this peat decreased faster than in deeper, denser peat. For this reason, a small increase in water table elevation may result in a large increase in water content, and thus upwards solute mobility. Conversely, in denser soil solute moves at a slower pace during saturated conditions, but due to its higher water retention capacity has a higher effective K_{unsat} and thus can better facilitate capillary rise in drier conditions.

A great deal of lateral and vertical heterogeneity was encountered during both saturated and unsaturated phases of this research. In deeper peat, the presence of the discontinuous high hydraulic conductivity layer at the ~125 cm depth was unexpected, and likely due to the unique depositional environment of this area. Variations in K_{sat} both between hummocks and hollows had a profound impact on the plume's final shape, and were responsible for the splitting of the plume into two distinct preferential flow pathways. In the unsaturated zone, an unexpected reversal of depth dependent dry bulk density, total porosity and effective porosity was encountered below 15 cm for all cores. This corresponded to visual observation of intact roots from vascular vegetation. Between three hummock mesocosms, lateral variations of soil properties in the top 15 cm had a profound impact on the rates of evaporation and upwards solute transport, despite the experiment taking place in a highly controlled environment. A highly porous upper 5 cm combined by much denser, less porous peat below provided the "ideal" conditions for solute breakthrough, which occurred in half the time as a core lacking this patterning.

The conclusions of this research can be used as a guiding tool in a real world contaminant release scenario. The short term lateral fate of a spilled contaminant, particularly in the case of a surficial spill, can be approximated using site water table gradient and depth, detailed topography, and meteorological conditions. This would be complicated by contaminant specific

behaviours, such as retardation due to sorption to the peat matrix, uptake of nutrients by site vegetation, or migration of Non Aqueous Phase Liquids (NAPLs) to the surface of the water table (LNAPLs such as hydrocarbons) or towards the bottom of the highly conductive zone (DNAPLs such as chlorinated solvents or extra heavy crude oil) (Freeze & Cherry, 1979).

Due to the extremely heterogeneous nature of peat deposits this information alone would be insufficient to properly track the vertical distribution of solute, particularly in a release below the ground surface. For this, the site-specific depositional environment and soil structure must be determined at a high enough density to account for the variability observed in laboratory conditions. Assumptions of depth- dependent trends, such as decreasing K, and total effective porosity with depth should be used with caution as they are not universally true. Further, care must be taken to ensure a sufficient number of cores are collected to be considered "site representative" in future experiments.

References

Andrus, R. E., Wagner, D. J., & Titus, J. E. (1983). Vertical zonation of Sphagnum mosses along hummock-hollow gradients. *Canadian Journal of Botany*, *61*(12), 3128–3139.

Baird, A. J. (1997). Field estimation of macropore functioning and surface hydraulic conductivity in a fen peat. *Hydrological Processes*, *3*, 287–295.

Baird, A. J., & Gaffney, S. W. (2000). Solute movement in drained fen peat : a field tracer study in a Somerset (UK) wetland. *Hydrological Processes*, *14*, 2489–2503. http://doi.org/1099-1085(20001015)14:14<2489::aid-hyp110>3.0.co;2-q

Baird, A. J., Milner, A. M., Blundell, A., Swindles, G. T., & Morris, P. J. (2016). Microform-scale variations in peatland permeability and their ecohydrological implications. *Journal of Ecology*, *104*(2), 531–544. http://doi.org/10.1111/1365-2745.12530

Beckwith, C. W., Baird, A. J., & Heathwaite, A. L. (2003). Anisotropy and depth-related heterogeneity of hydraulic conductivity in a bog peat. I: laboratory measurements. *Hydrological Processes*, *17*(1), 89–101. http://doi.org/10.1002/hyp.1116

Boelter, D. H. (1969). Physical properties of peats as related to degree of decomposition. *Soil Science Society of America Journal*, *33*(4), 606–609. doi:10.2136/sssaj1969.03615995003300040033x

Boelter, D. H. (1965). Hydraulic conductivty of peats *Soil Science*, *100*(4), 227–231.

Brewer, R. (1965). Fabric and mineral analysis of soils. *Soil Science*, *100*(1), 73.

Carey, S. K., Quinton, W. L., & Goeller, N. (2007). Field and laboratory estimates of pore size properties and hydraulic characteristics for sub-arctic organic soils. *Hydrological Processes*, *2274*(November 2008), 2267–2274. http://doi.org/10.1002/hyp

Deiss, J., Byers, C., Clover, D., D'Amore, D., Love, A., Menzies, M., Powell, J., Walter, M. T. (2004). Transport of lead and diesel fuel through a peat soil near Juneau, AK: a pilot study. *Journal of Contaminant Hydrology*, *74*(1–4), 1–18. http://doi.org/10.1016/j.jconhyd.2004.02.003

Environment Canada. (2015a). Canadian climate normals 1791-2000: Moosonee. Retrieved 26/10/2015 from Environment Canada http://www.climate.weatheroffice.gc.ca/climate_normals/

Environment Canada. (2015b). Canadian Climate Normals 1971-2000: Lansdowne House. Retrieved 26/10/2015 from Environment Canada http://www.climate.weatheroffice.gc.ca/climate_normals/

Freeze, R. A., & Cherry, J. A. (1979) *Groundwater.* Prentice-Hall, Englewood Cliffs, NJ

Glaser, P. H., Hansen, B. C. S., Siegel, D. I., Reeve, A. S., & Morin, P. J. (2004). Rates, pathways and drivers for peatland development in the Hudson Bay Lowlands, Northern Ontario, Canada. *Journal of Ecology*, *92*(6), 1036–1053. http://doi.org/10.2307/3599747

Gnatowski, T., Szatyłowicz, J., Brandyk, T., & Kechavarzi, C. (2010). Hydraulic properties of fen peat soils in Poland. *Geoderma*, *154*(3–4), 188–195. http://doi.org/10.1016/j.geoderma.2009.02.021

Goetz, J. D., & Price, J. S. (2015). Role of morphological structure and layering of Sphagnum and Tomenthypnum mosses on moss productivity and evaporation rates. *Canadian Journal of Soil Science*, *95*, 109–124.

Gorham, E. (2008). Northern Peatlands : Role in the carbon cycle and probable responses to climatic warming. *Ecological Applications*, *1*(2), 182–195.

Hayward, P. M., & Clymo, R. S. (1982). Profiles of water content and pore size in Sphagnum and peat, and their relation to peat bog ecology. *Proceedings of the Royal Society B: Biological Sciences*, *215*(1200), 299–325. http://doi.org/10.1098/rspb.1982.0044

Hilhorst, M. A. (2000). A pore water conductivity sensor. *Soil Science Society of America Journal*, *64*(6), 1922–1925.

Hoag, S. R., & Price, J. (1997). The effects of matrix diffusion on solute transport and retardation in undisturbed peat in laboratory columns. *Journal of Contaminant Hydrology*, *28*, 193–205.

Hoag, S. R., & Price, S. J. (1995). A field-scale, natural gradient solute transport experiment in peat at a Newfoundland blanket bog. *Journal of Hydrology*, *172*(1–4), 171–184. http://doi.org/10.1016/0022-1694(95)02696-M

Holden, J. (2009). Flow through macropores of different size classes in blanket peat. *Journal of Hydrology*, *364*(3–4), 342–348. http://doi.org/10.1016/j.jhydrol.2008.11.010

Hvorslev, M. J. (1951). *Time Lag and Soil Permeability in Ground-Water Observations* (Vol. Waterways Experimental Station Bulletin 36). Vicksburg, Mississippi: US Army Corps of Engineers.

Hydrologic Consultants of Colorado. (2004). *Dewatering of the Victor Diamond Mine Project. Predicted Engineering, Cost, and Environmental Factors*.

Ingram, H. A. P. (1978). Soil Layers in mires: function and terminology. *Journal of Soil Science*, *29*(2), 224–227. http://doi.org/10.1111/j.1365-2389.1978.tb02053.x

Leclair, M. M. (2015). *The hydrological interactions within a mine impacted peatland, James Bay Lowland, Canada*. (Master of Science),University of Waterloo, Waterloo, Ontario.

Martini, I. (1981). Morphology and sediments of the emergent Ontario coast of James Bay, Canada. *Geografiska Annaler: Series A, Physical Geography*, *63*(1), 81–94.

McCarter, C. P. R. (2016). *The Hydrochemical Fate and Transport of Treated Domestic Wastewater Contaminants During a Wastewater Polishing Experiment in a Sub-Arctic Ladder Fen Peatland*. (Doctoral Dissertation) University of Waterloo, Waterloo, Ontario.

McCarter, C. P. R., & Price, J. S. (2014). Ecohydrology of Sphagnum moss hummocks:

mechanisms of capitula water supply and simulated effects of evaporation. *Ecohydrology*, *7*(1), 33–44. http://doi.org/10.1002/eco.1313

McCarter, C. P. R., & Price, J. S. (2017a). Experimental hydrological forcing to illustrate water flow processes of a sub-arctic ladder fen peatland. *Hydrological Processes*. http://doi.org/10.1002/hyp.11127

McCarter, C. P. R., & Price, J. S. (2017b). The transport dynamics of chloride and sodium in a ladder fen during a continuous wastewater polishing experiment. *Journal of Hydrology (In Review)*.

McDonald, B. (1989). *Glacial and interglacial stratigraphy, Hudson Bay Lowland. In Quaternary Geology of Canda and Greeland, Geology of Canada*. (R. Fulton, Ed.). Ottawa: Geological Survey of Canada.

National Wetlands Working Group (1997). *The Canadian Wetland Classification System-Second Edition*. University of Waterloo, Waterloo, Ontario

Ours, D. P., Siegel, D. ., & H. Glaser, P. (1997). Chemical dilation and the dual porosity of humified bog peat. *Journal of Hydrology*, *196*(1–4), 348–360. http://doi.org/10.1016/S0022-1694(96)03247-7

Perras, E. (2015). *Hydrological and Geochemical Implications of Aquifer Depressurization on Expansive Peatland Systems in the Hudson/ James Bay Lowlands*. (Master of Science) University of Waterloo, Waterloo, Ontario.

Pouliot, R., Rochefort, L., & Graf, M. (2012). Impacts of oil sands process water on fen plants: implications for plant selection in required reclamation projects. *Environmental Pollution*, *167*, 132–137. http://doi.org/10.1016/j.envpol.2012.03.050

Price, J. S., & Ketcheson, S. J. (2009). Water relations in cutover peatlands. *Carbon Cycling in Northern Peatlands*, 277–287. http://doi.org/10.1029/2008GM000827

Price, J. S., & Maloney, D. A. (1994). Hydrology of a patterned bog-fen complex in southeastern Labrador, Canada. *Nordic Hydrology, 25*, 313-330

Price, J. S., & Whittington, P. N. (2010). Water flow in Sphagnum hummocks: Mesocosm measurements and modelling. *Journal of Hydrology*, *381*(3–4), 333–340. http://doi.org/10.1016/j.jhydrol.2009.12.006

Price, J. S., Whittington, P. N., Elrick, D. E., Strack, M., Brunet, N., & Faux, E. (2008). A Method to determine unsaturated hydraulic fonductivity in living and undecomposed Sphagnum moss. *Soil Science Society of America Journal*, *72*(2), 487. http://doi.org/10.2136/sssaj2007.0111N

Price, S. J. (1994). Sources and sinks of sea salt in a newfoundland blanket bog. *Hydrological Processes*, *8*(2), 167–177.

Price, S. J., & Woo, M. K. (1988). *Wetlands as waste repositories? : Solute transport in peat.* Paper presented at the Proc. National Student Conference on Northern Studies, Ottawa.

Priestley, C. H. B., & Taylor, R. J. (1972). On the Assessment of Surface Heat Flux and Evaporation Using Large-Scale Parameters. *Monthly Weather Review*, *100*(2), 81–92. http://doi.org/10.1175/1520-0493(1972)100<0081:OTAOSH>2.3.CO;2

Quinton, W. L., Hayashi, M., & Pietroniro, A. (2003). Connectivity and storage functions of channel fens and flat bogs in northern basins. *Hydrological Processes*, *17*(18), 3665–3684. http://doi.org/10.1002/hyp.1369

Quinton, W. L., Price, J., Rezanezhad, F., & Heck, R. (2009). Measuring physical and hydraulic properties of peat from X-ray tomography. *Geoderma*, *153*(1–2), 269–277. http://doi.org/10.1016/j.geoderma.2009.08.010

Rezanezhad, F. ., Price, S. J., Quinton, L. W., Lennartz, B., Milojevic, T., & Van Cappellen, P. (2016). Structure of peat soils and implications for water storage, flow and solute transport: A review update for geochemists. *Chemical Geology*, *429*, 75–84. http://doi.org/http://dx.doi.org/10.1016/j.chemgeo.2016.03.010

Rezanezhad, F., Price, J. S., & Craig, J. R. (2012). The effects of dual porosity on transport and retardation in peat: A laboratory experiment. *Canadian Journal of Soil Science*, *92*(5), 723–732. http://doi.org/10.4141/cjss2011-050

Rezanezhad, F., Quinton, W. L., Price, J. S., Elliot, T. R., Elrick, D., & Shook, K. R. (2010). Influence of pore size and geometry on peat unsaturated hydraulic conductivity computed from 3D computed tomography image analysis. *Hydrological Processes*, *24*(21), 2983–2994. http://doi.org/10.1002/hyp.7709

Rezanezhad, F., Quinton, W. L., Price, J. S., Elrick, D., Elliot, T. R., & Heck, R. J. (2009). Examining the effect of pore size distribution and shape on flow through unsaturated peat using 3-D computed tomography. *Hydrology and Earth System Sciences Discussions*, *6*(3), 3835–3862. http://doi.org/10.5194/hessd-6-3835-2009

Riley, J. L. (2011). *Wetlands of the Ontario Hudson Bay lowland: A Regional Overview*. *Nature Conservancy of Canada: Toronto, Ontario*. http://doi.org/10.1017/CBO9780511542091.005

Robroek, B. J. M., Limpens, J., Breeuwer, A., & Schouten, M. G. C. (2007). Effects of water level and temperature on performance of four Sphagnum mosses. *Plant Ecology*, *190*(1), 97–107. http://doi.org/10.1007/s11258-006-9193-5

Schlotzhauer, S. M., & Price, J. S. (1999). Soil water flow dynamics in a managed cutover peat field , Quebec : Field and laboratory investigations. *Water Resources Research*, *35*(12), 3675–3683.

Siegel, D., & Glaser, P. (1987). Groundwater flow in a bog-fen *The Journal of Ecology*, *75*, 743–754.

Simhayov, R. (2017). *Chemical Characterization of construction materials and solute transport in peat from the Nikanotee constructed fen watershed in the Athabasca oil sands region, Alberta, Canada (Doctoral thesis)*. University of Waterloo, Waterloo, Canada.

Ulanowski, T. A., & Branfireun, B. a. (2013). Small-scale variability in peatland pore-water biogeochemistry, Hudson Bay Lowland, Canada. *The Science of the Total Environment, 454–455*, 211–218. http://doi.org/10.1016/j.scitotenv.2013.02.087

Vervoort, R. W., & Cattle, S. R (2003) Linking hydraulic conductivity and tortuosity parameters to pore space geometry and pore-size distribution. *Journal of Hydrology, 272,* 36-49

Weiss, R., Alm, J., Laiho, R., & Laine, J. (1998). Modeling moisture retention in peat soils. *Soil Sci. Soc. Am. J., 62*(2), 305–313. http://doi.org/10.2136/sssaj1998.03615995006200020002x

Whittington, P., & Price, J. S. (2012). Effect of mine dewatering on the peatlands of the James Bay Lowland: The role of marine sediments on mitigating peatland drainage. *Hydrological Processes*, *27*(March), 1845–1853. http://doi.org/10.1002/hyp.9858

Appendix A

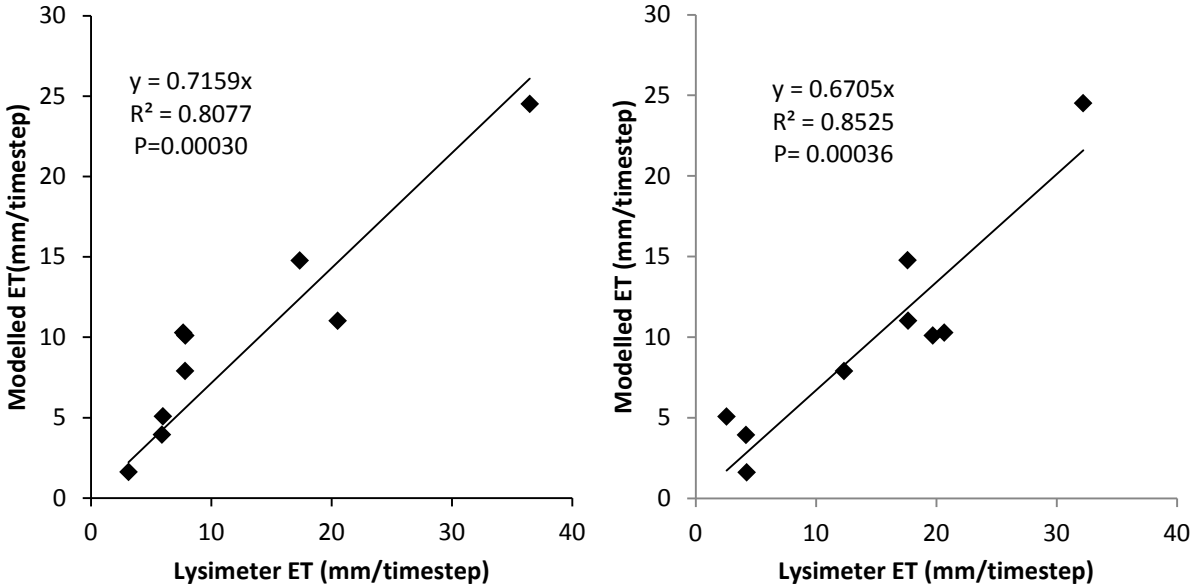

Figure A-1 Hummock (left) and hollow (right) fitted ANOVA linear regression between lysimeter evapotranspiration and that calculated using the Priestley-Taylor method. α values are the slopes of the fitted lines when the y-intercept is set to zero.

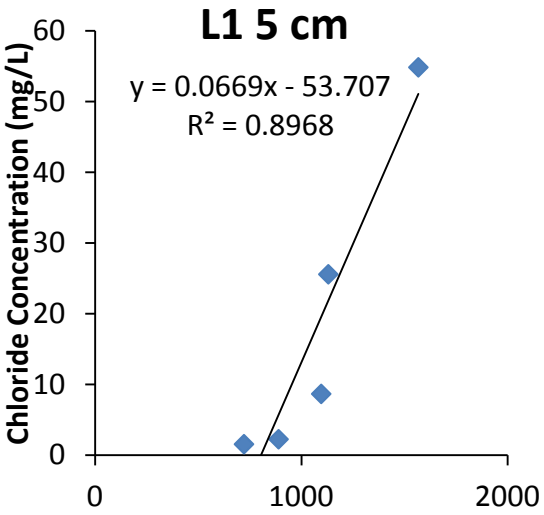
L1 5 cm
y = 0.0669x - 53.707
R² = 0.8968
Chloride Concentration (mg/L)
0
10
20
30
40
50
60
0
1000
2000

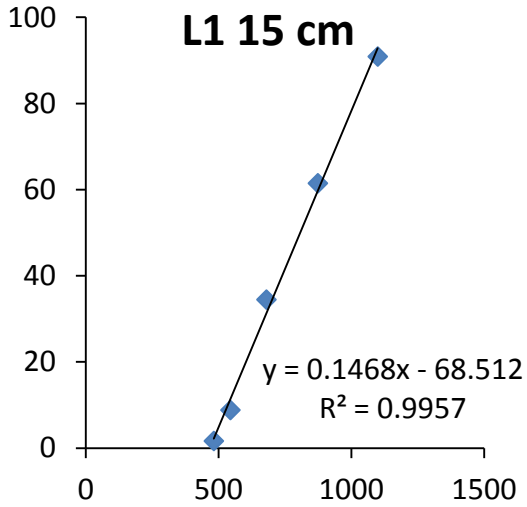
L1 15 cm
y = 0.1468x - 68.512
R² = 0.9957
0
20
40
60
80
100
0
500
1000
1500

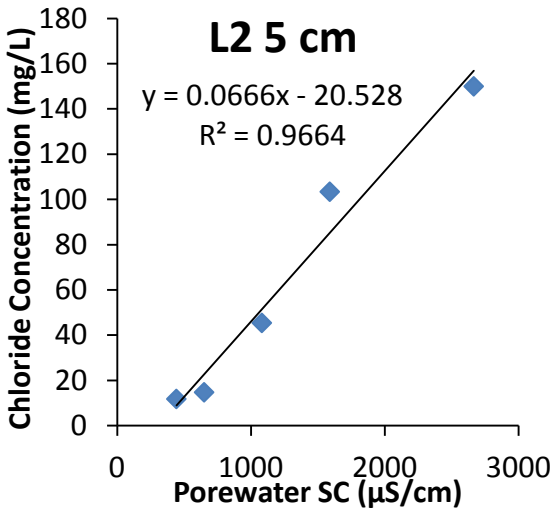
L2 5 cm
y = 0.0666x - 20.528
R² = 0.9664
Chloride Concentration (mg/L)
0
20
40
60
80
100
120
140
160
180
0
1000
2000
3000
Porewater SC (µS/cm)

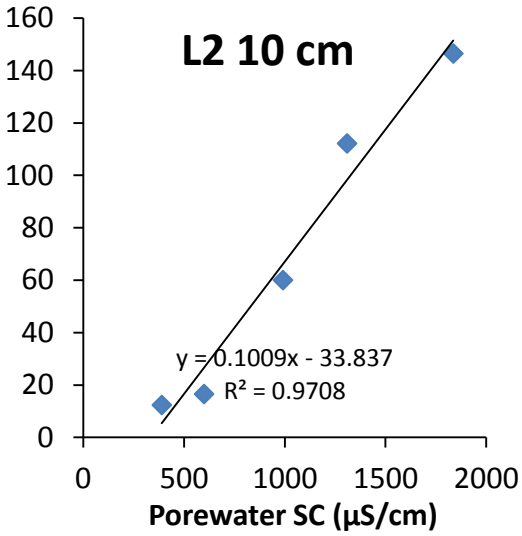
L2 10 cm
y = 0.1009x - 33.837
R² = 0.9708
0
20
40
60
80
100
120
140
160
0
500
1000
1500
2000
Porewater SC (µS/cm)

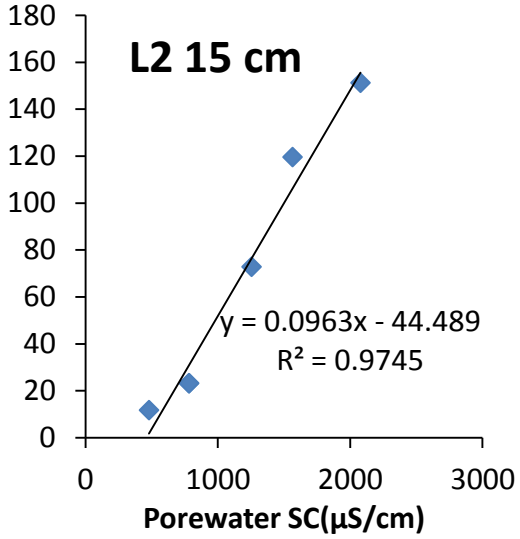
L2 15 cm
y = 0.0963x - 44.489
R² = 0.9745
0
20
40
60
80
100
120
140
160
180
0
1000
2000
3000
Porewater SC(µS/cm)

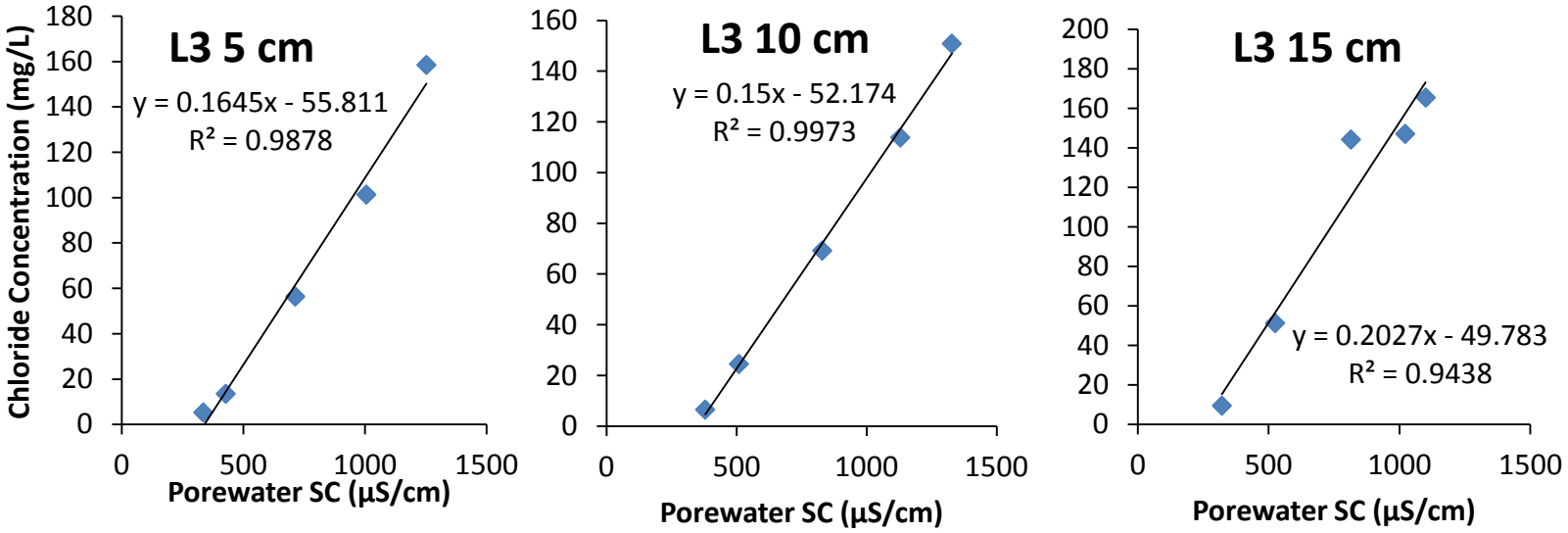

Figure A.2 Fitted relationships between measured porewater Specific Conductance and chloride concentrations at a given sampling depth at cores L1, L2, and L3, including equations used to transform SC data to Cl^- concentration data.